15 - 19 June 2026
Kraków, Poland

FRINGE 2026

Kinematics, Dynamics, and Seismic Potential of the Tianshan from Sentinel-1 InSAR & GNSS

Fengnian Chang[1,2], Andy Hooper[2], John Elliott[2], Jin Fang[2], Shaochun Dong[1], Hongwei Yin[1]

[1]School of Earth Sciences and Engineering, Nanjing University, Nanjing 210023, China

[2]COMET, School of Earth, Environment and Sustainability, University of Leeds; Leeds, UK

18 June 2026

Outline

1 Interseismic Velocity and Strain Rate

2 Slip Deficit Rate and Seismic Potential

3 From Kinematics to Dynamics

Tectonic Background

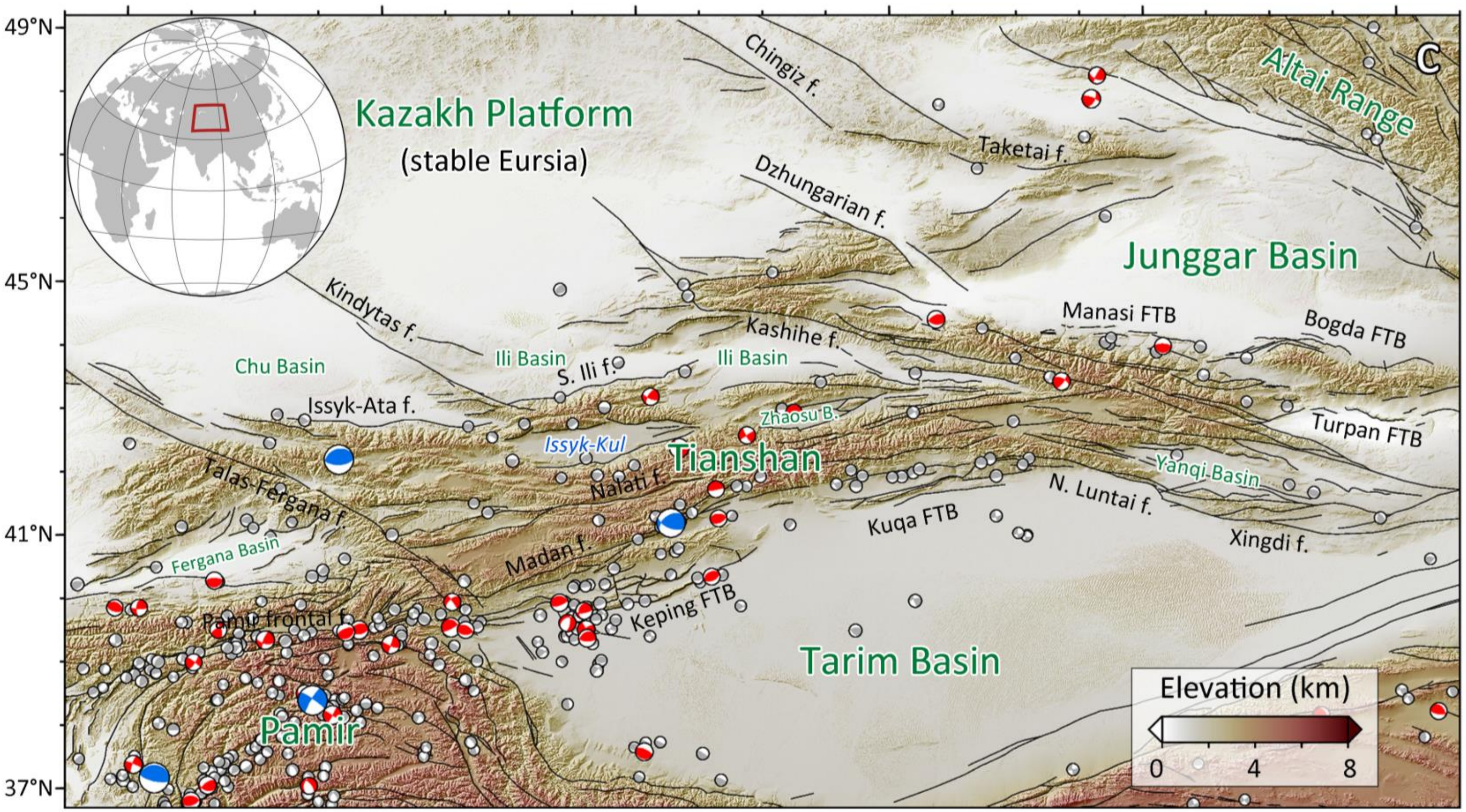

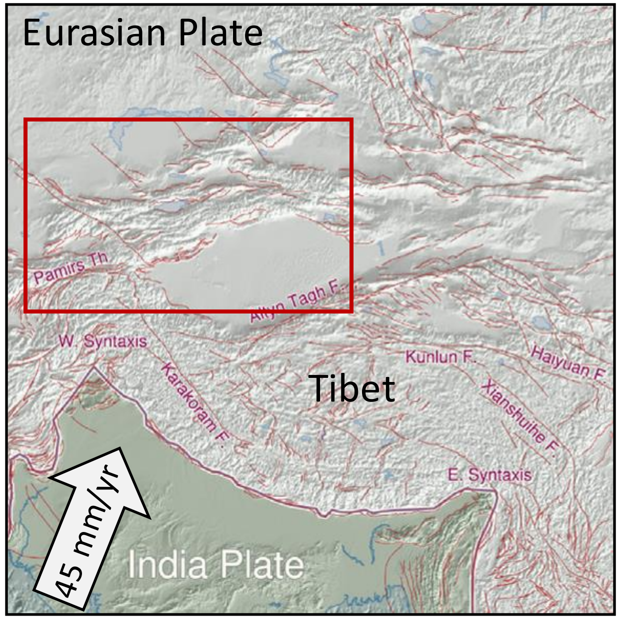

Motivation - Science & Society

- Kinematics, Dynamics, and Seismic Risk
- Resources and Energy (Oil/Gas/Minerals)
- Infrastructure (Energy pipelines/Railway)

- Tectonically active (~20 mm/yr, about half the plate convergence rate)
- Frequent earthquakes (over 100 Mw ≥ 6 earthquakes)

InSAR Time Series Analysis

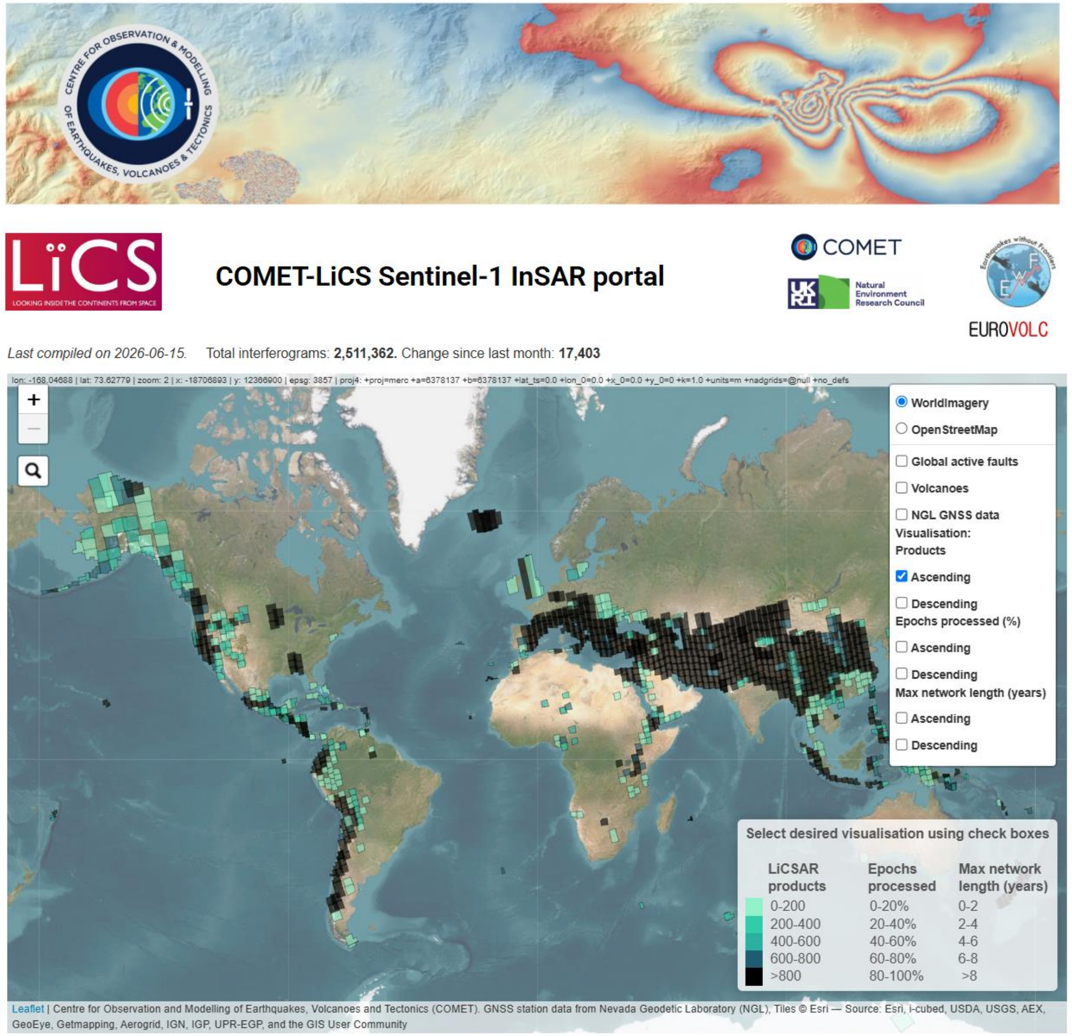

Real-time standard interferogram products

LiCSAR data: 21 tracks/92 frames/~100,000 ifgs/2014-2024

(Lazecký et al., 2020)

Time Series Analysis - LiCSBAS (Morishita et al., 2020)

InSAR

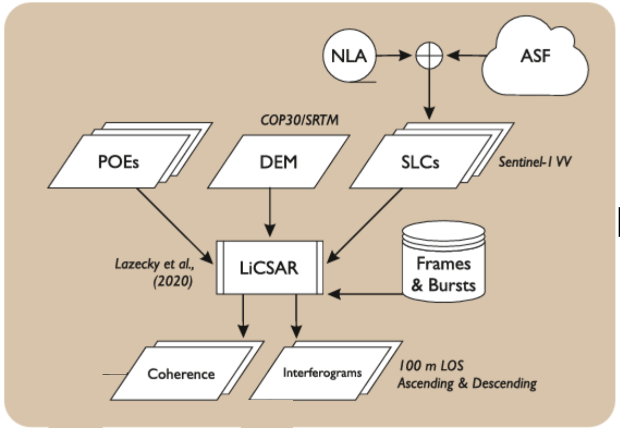

Time series

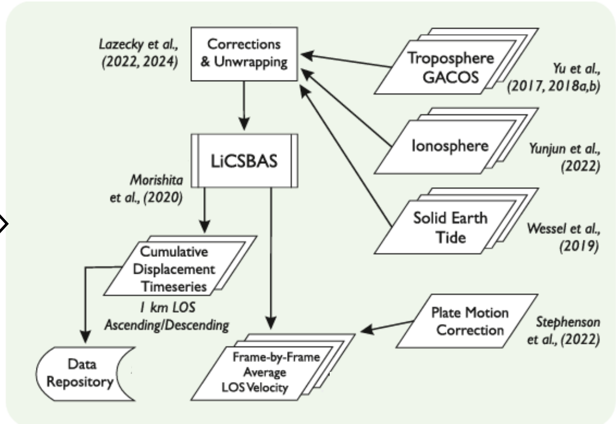

(Elliott et al., 2026)

Correction of Non-Tectonic Errors

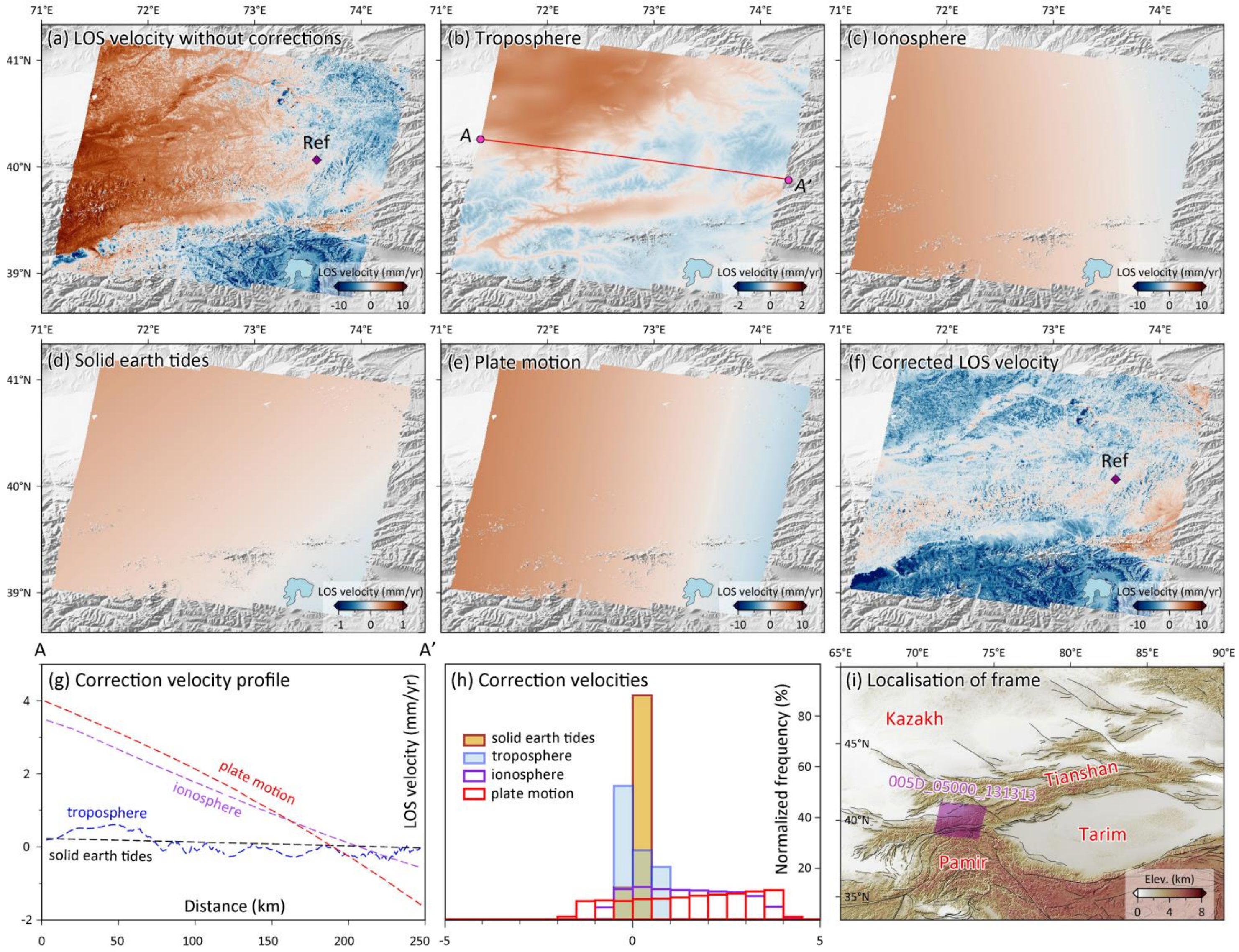

Application of corrections on example frame 005D_05000_131313

- Troposphere (GACOS) (Yu et al., 2018)
- Ionosphere (Zhang et al., 2022)
- Solid earth tide (Earth tide tool in GMT) (Wessel et al., 2019)
- Plate motion (Stephenson et al., 2022)

Co-seismic deformation correction

COMET
UNIVERSITY OF LEEDS

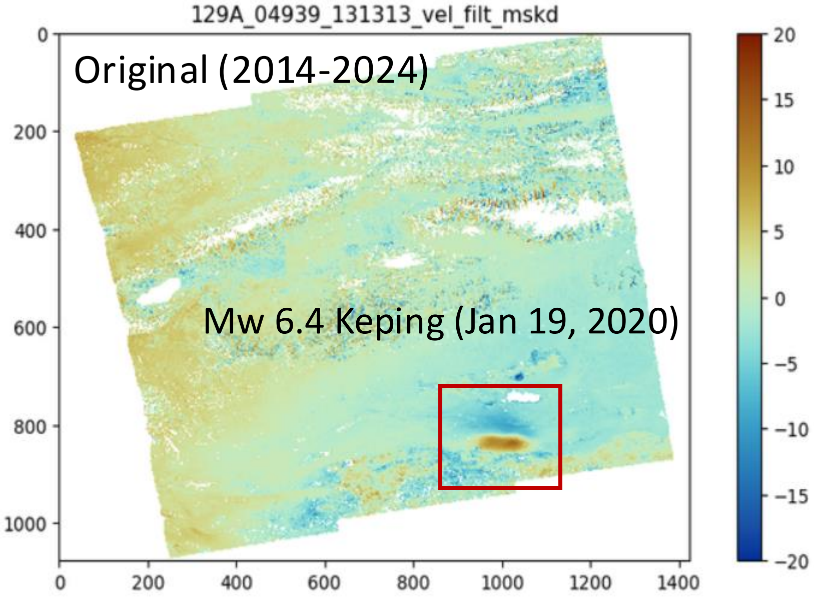

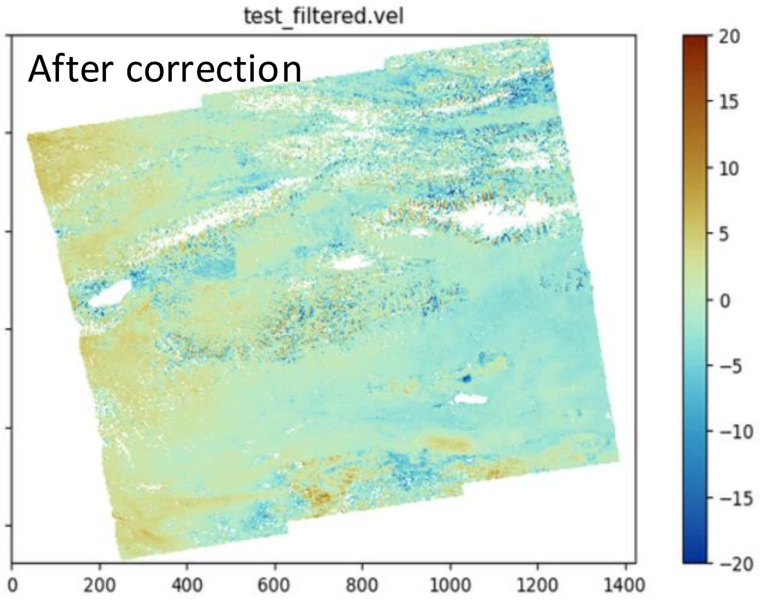

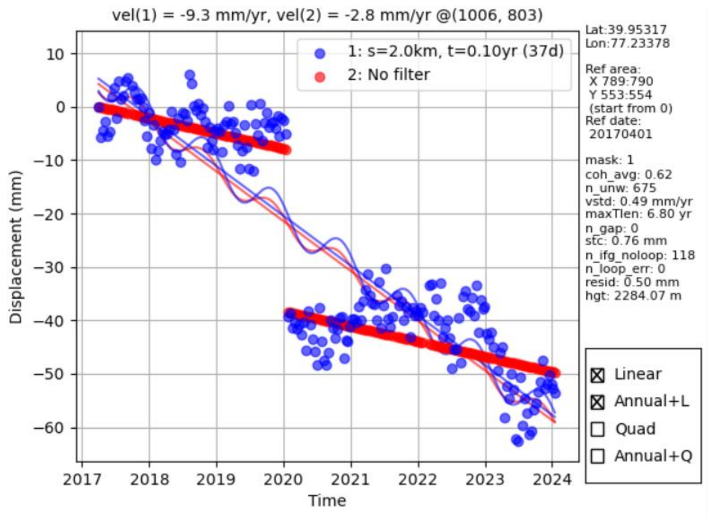

Fitting a Step Function (pixelwise)

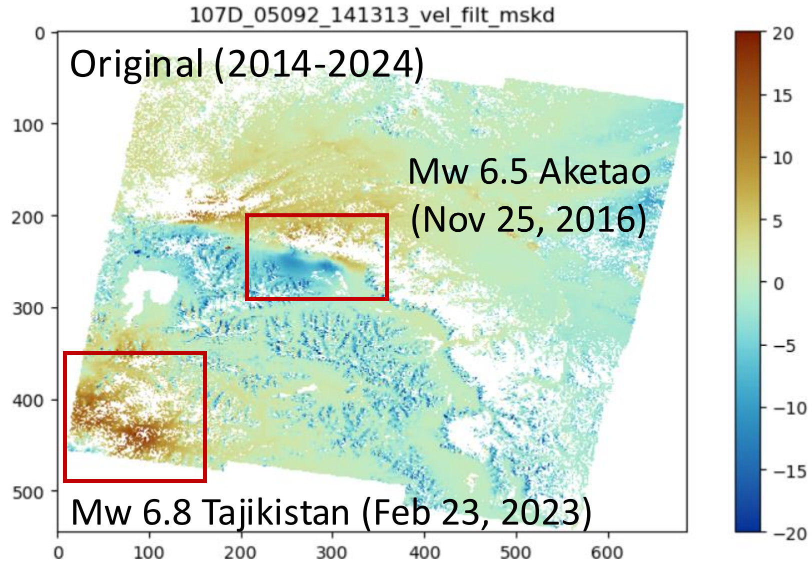

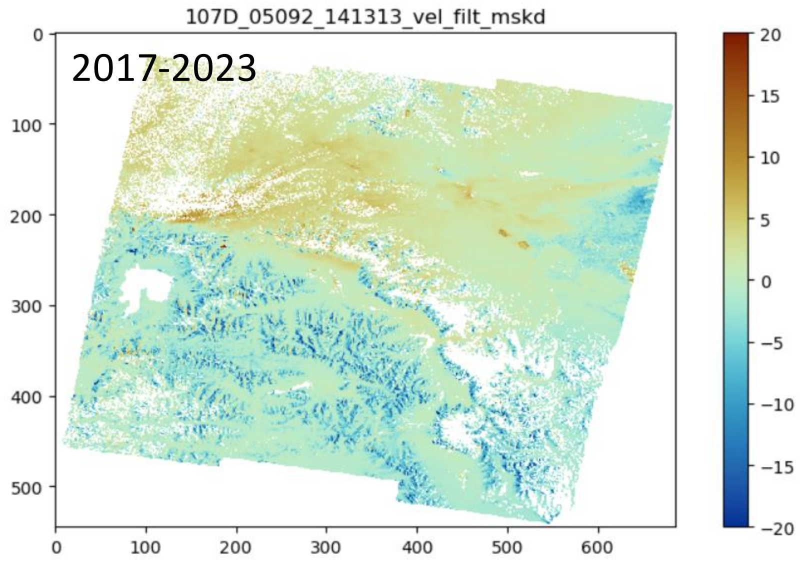

Time Series Truncation

(After/Before Earthquake)

6 earthquakes, 21 frames

Line-of-Sight Velocities

COMET
UNIVERSITY OF LEEDS

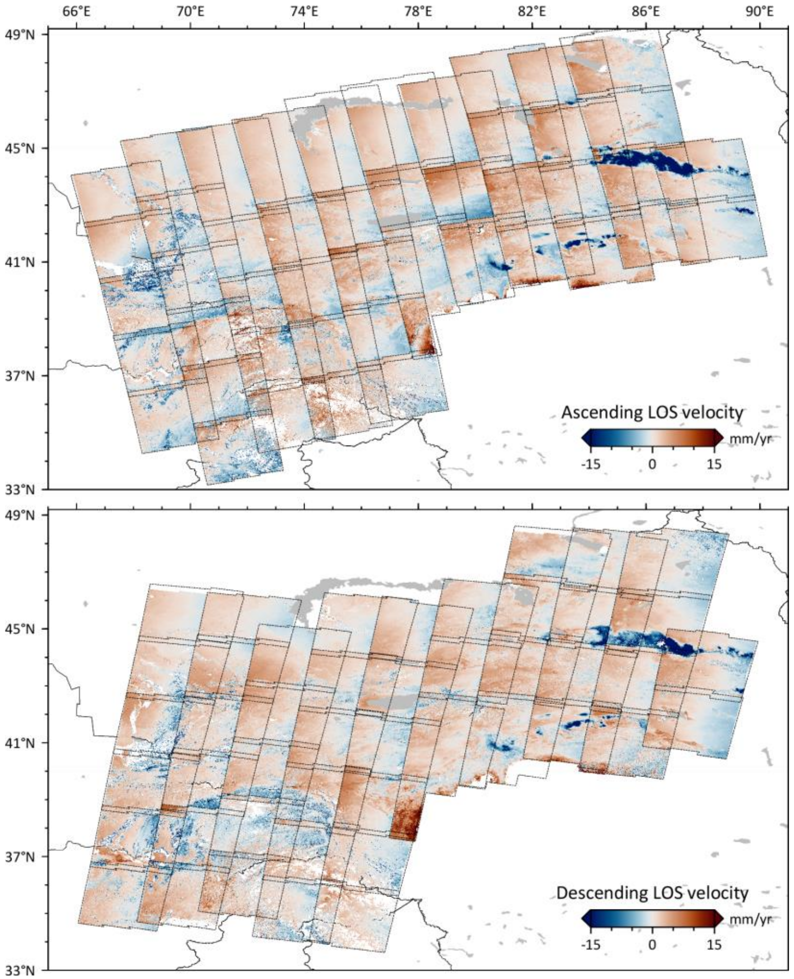

LOS Velocities
(Referenced separately)

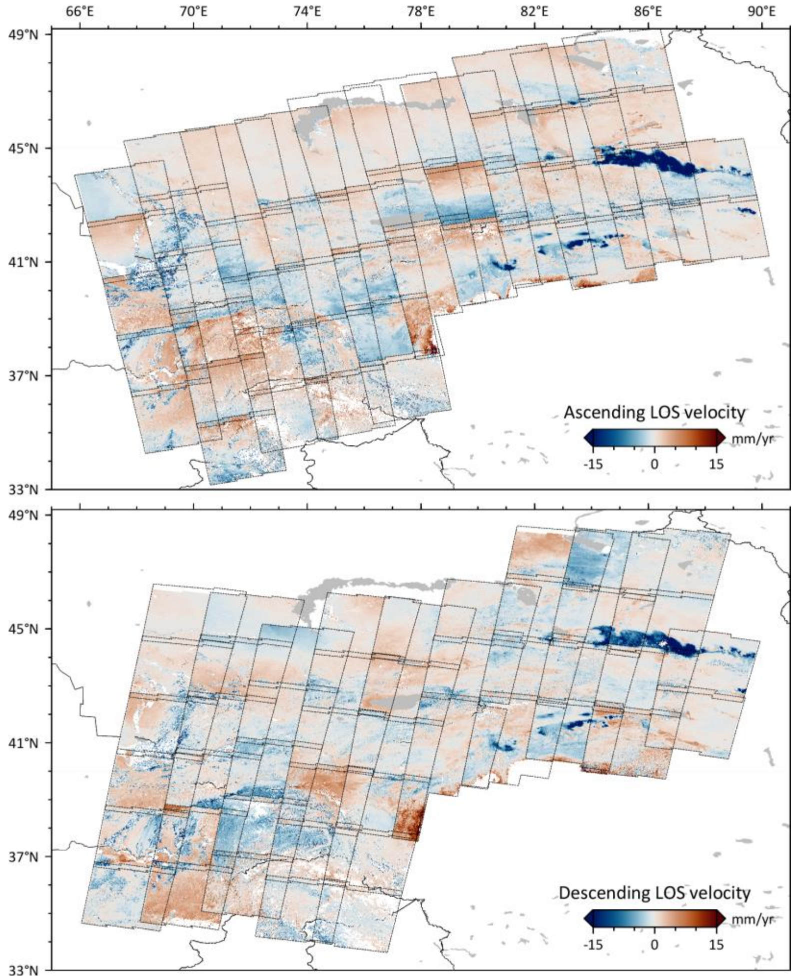

LOS Velocities after corrections
(Referenced separately)

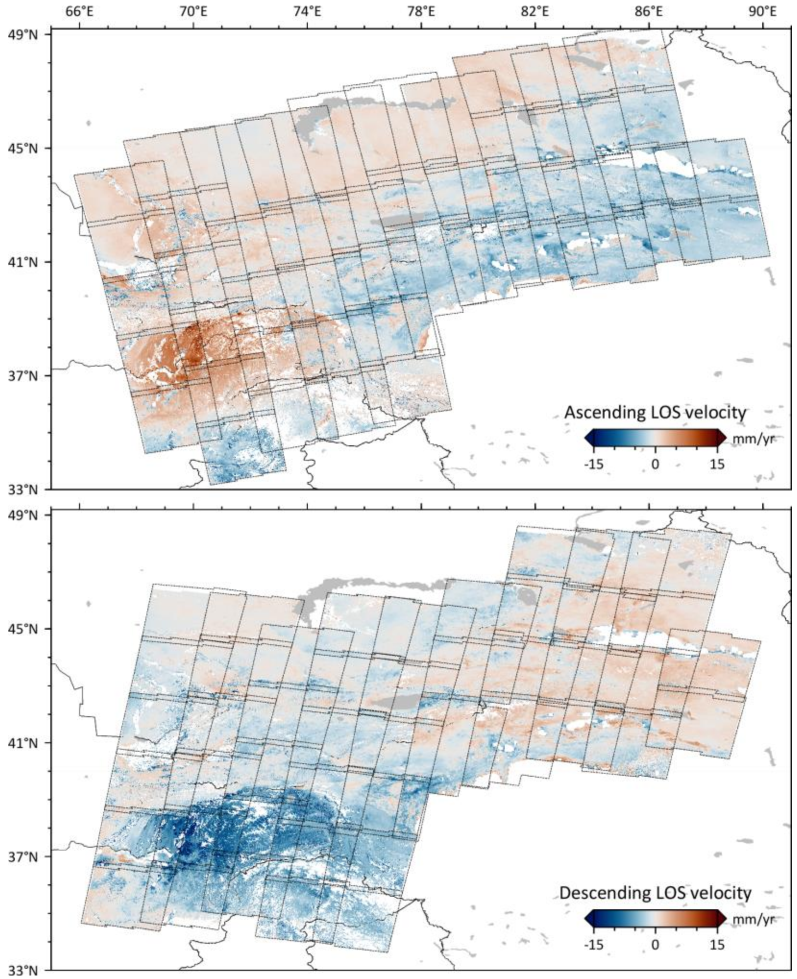

Eura-fixed LOS
(Align with GNSS reference frame)
Mask threshold (15 mm/yr)

GNSS Velocity Fields

COMET

UNIVERSITY OF LEEDS

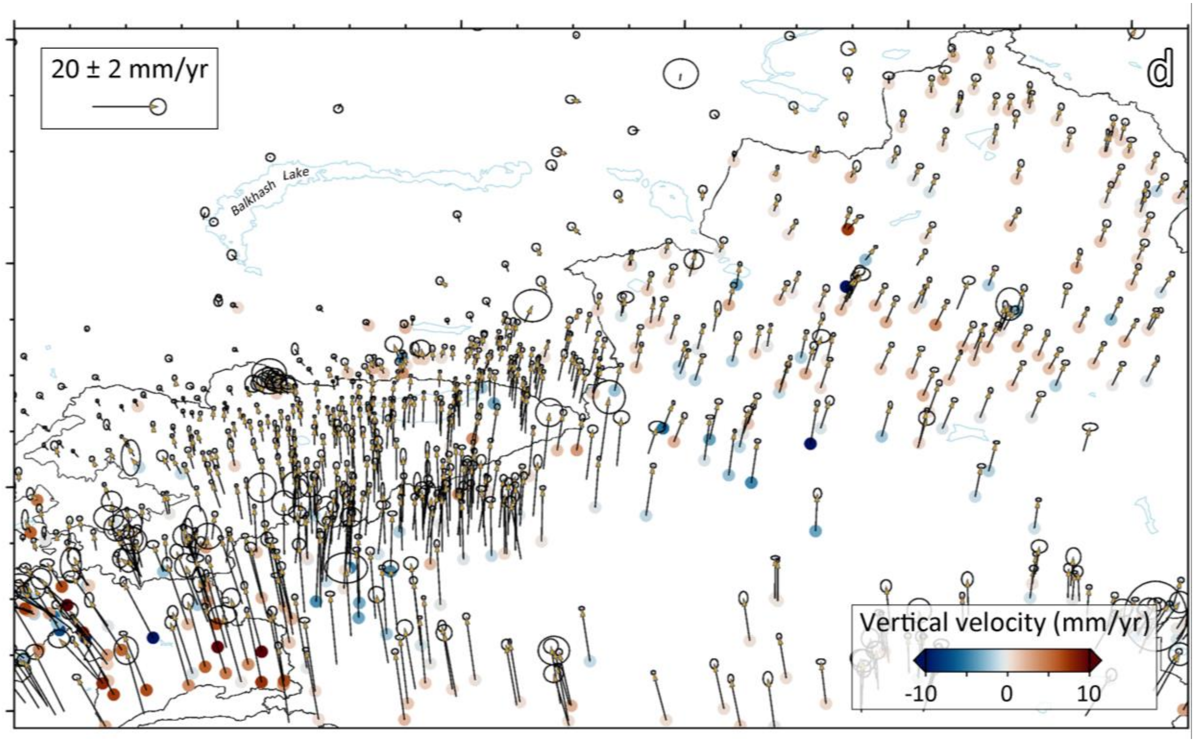

~1,000 GNSS velocity vector (2D+3D) with respect to the ITRF2014 Eurasia-fixed reference frame.

From AHB GNSS Dataset (Elliott et al., 2026)

Compile Published Literature Datasets   Automatic Outlier Detection/Removal   Alignment Euler-pole Rotation   GNSS Velocity

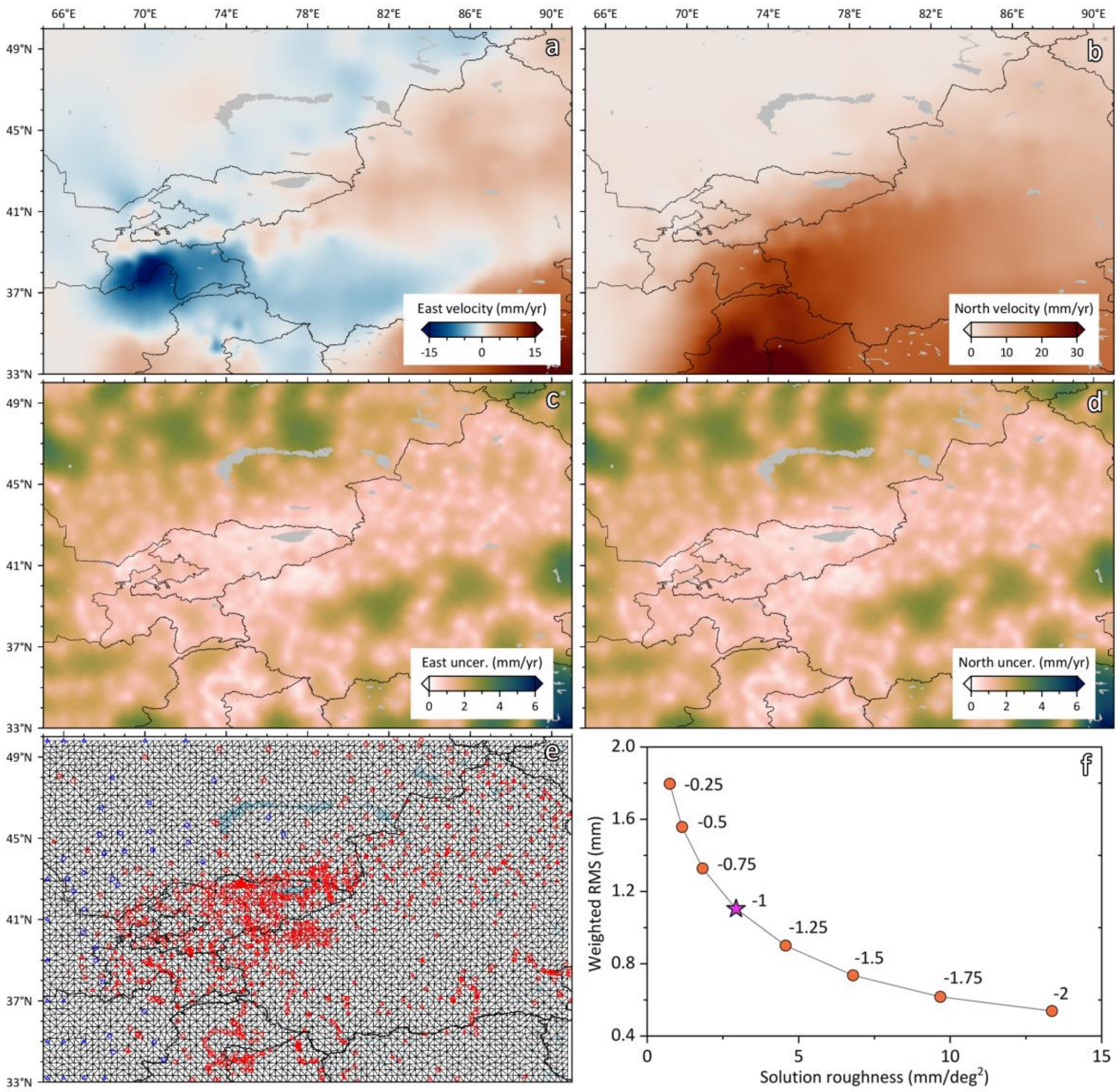

VELMAP Interpolation (Wang & Wright, 2012)

Velocity Decomposition

Asc. + Des. + GNSS north $\xrightarrow{\text{WLS}}$ East and Vertical

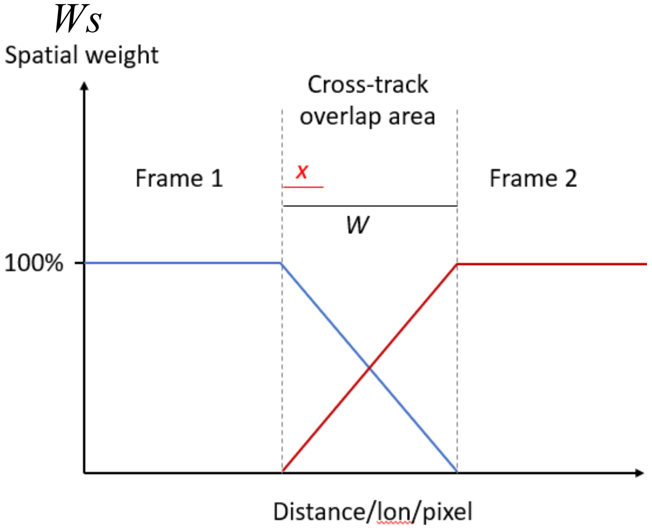

$$\omega_L(x) = \frac{W - x}{W}, \quad \omega_R(x) = \frac{x}{W}$$

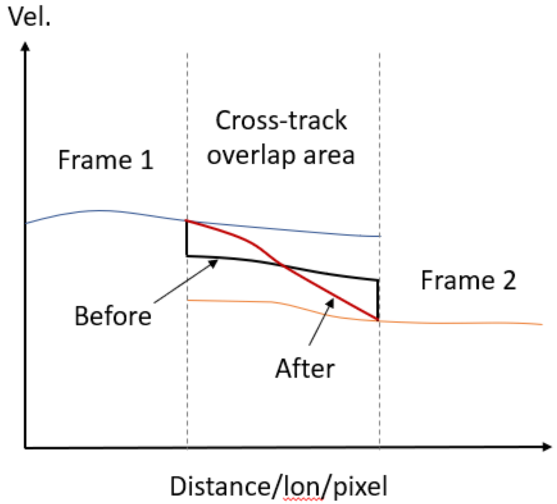

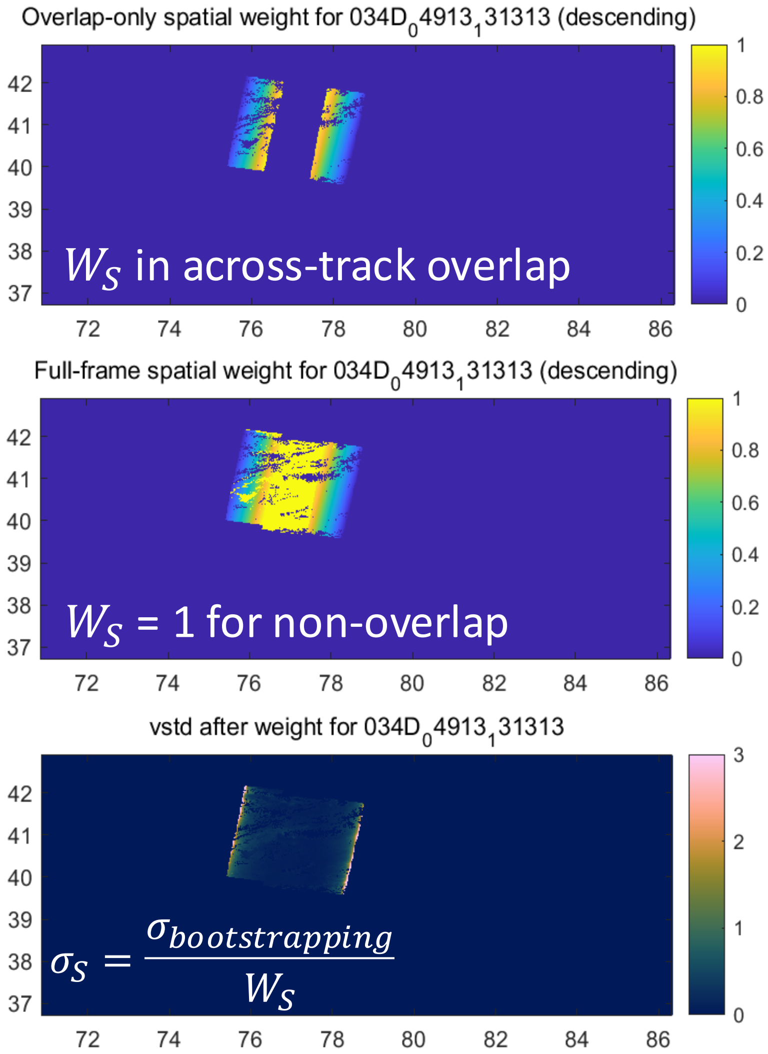

Combining formal uncertainty ($\sigma_{bootstrapping}$) with W_S

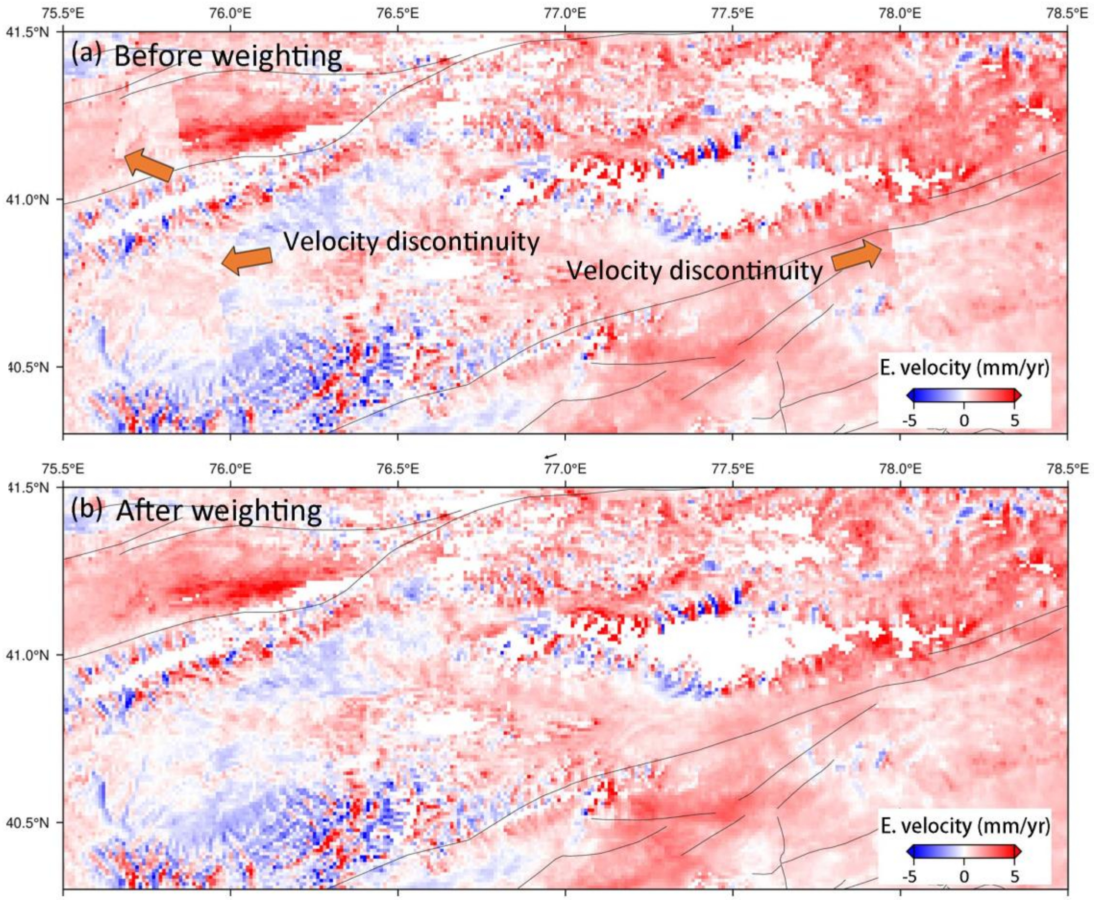

Comparison of velocity before and after spatial weighting

Interseismic Velocity

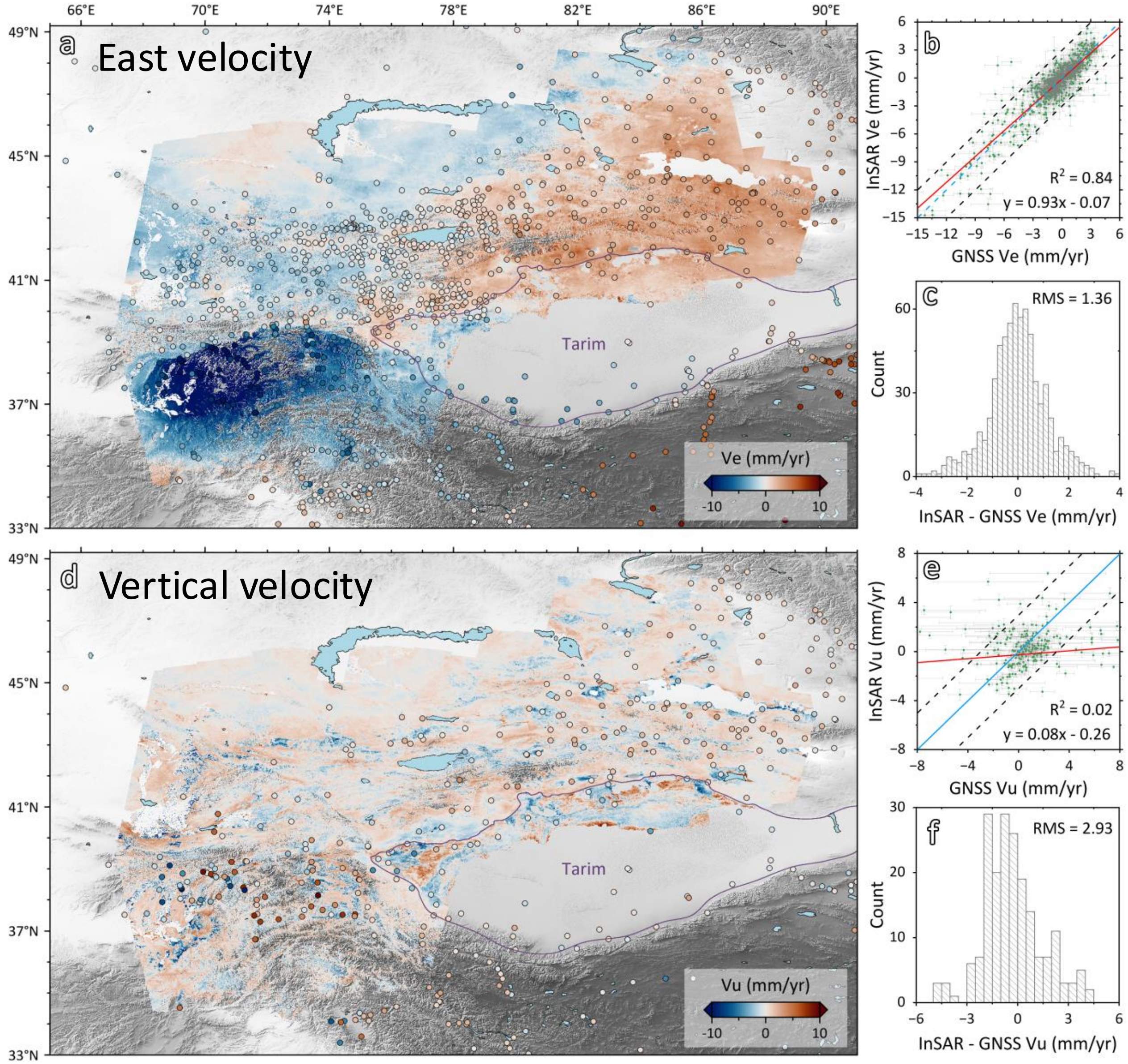

500 m resolution, ~2 million km^2

- East-west velocity shows good agreement with GNSS
- Vertical velocity is more difficult to interpret
- Vertical velocity is suppressed when aligned with GNSS

Uncertainty Estimation from Redundant Observations

4 independent LOS observations

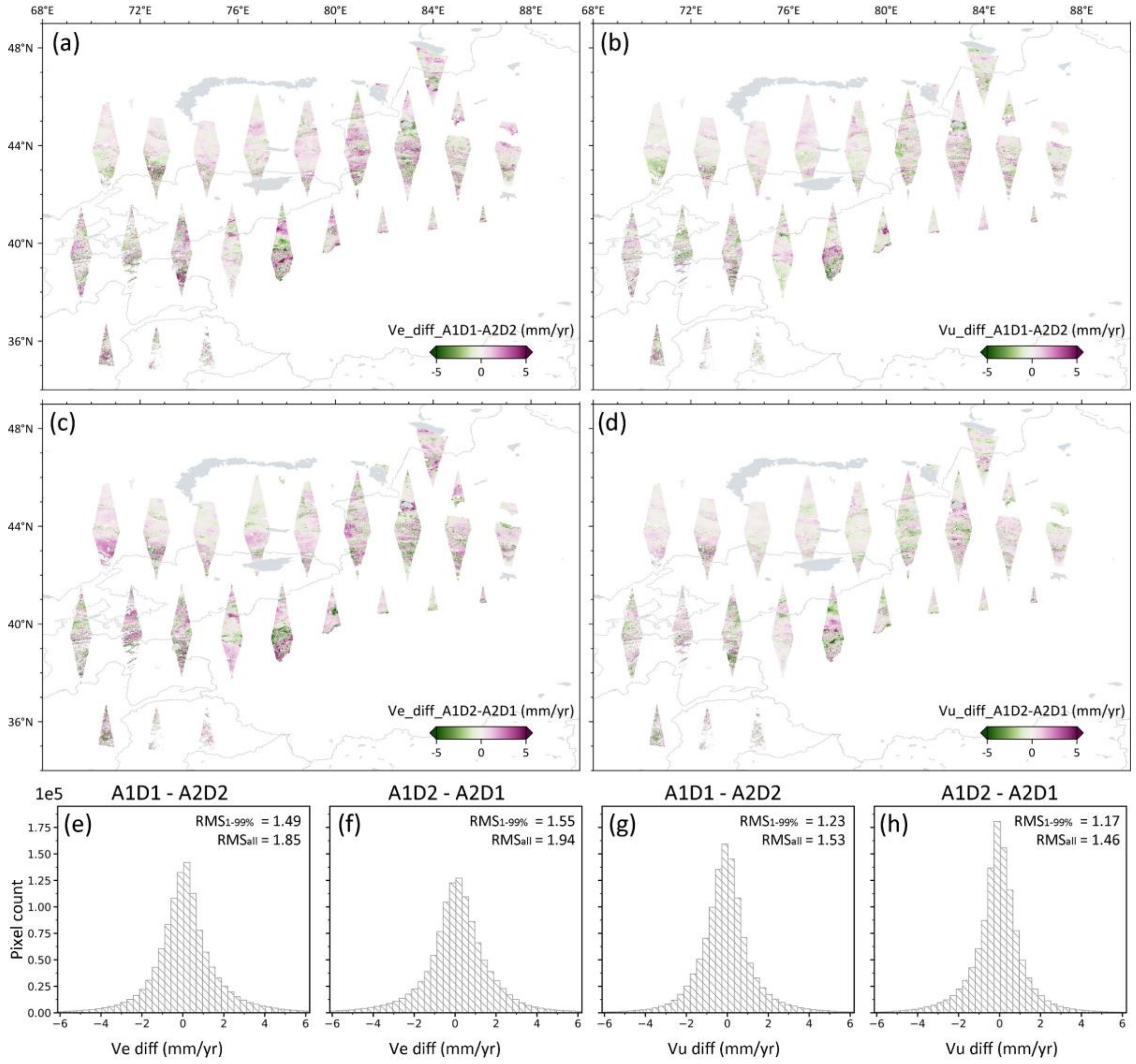

sig Ve ≈ 1.1 mm/yr sig Vu ≈ 0.9 mm/yr

3 independent LOS observations

(Wright et al., 2026; Elliott et al., 2026)

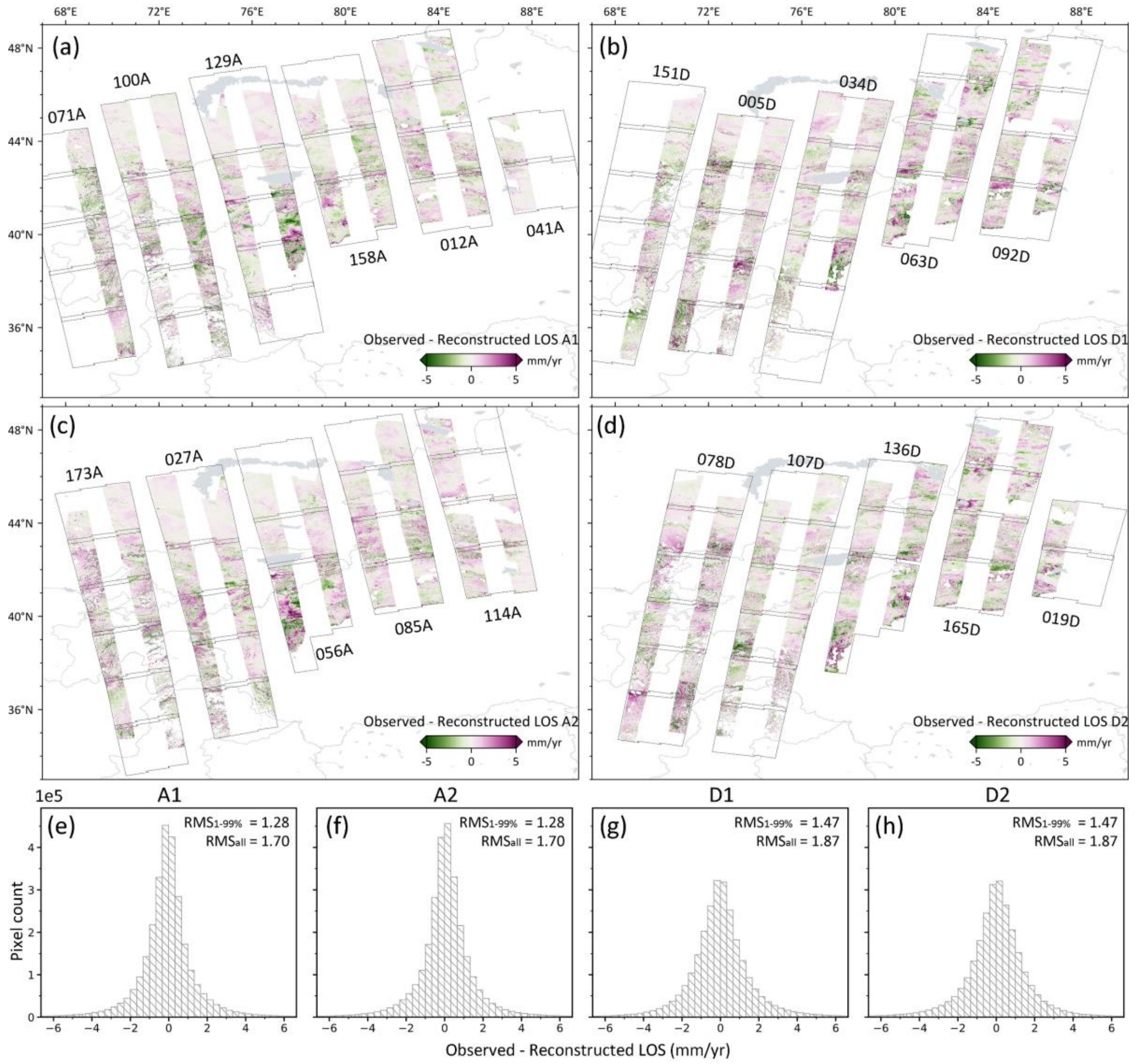

sig V_{los_a} ≈ 0.8 mm/yr sig V_{los_d} ≈ 1.1 mm/yr

Strain Rate Calculation – Velocity filtering

COMET UNIVERSITY OF LEEDS

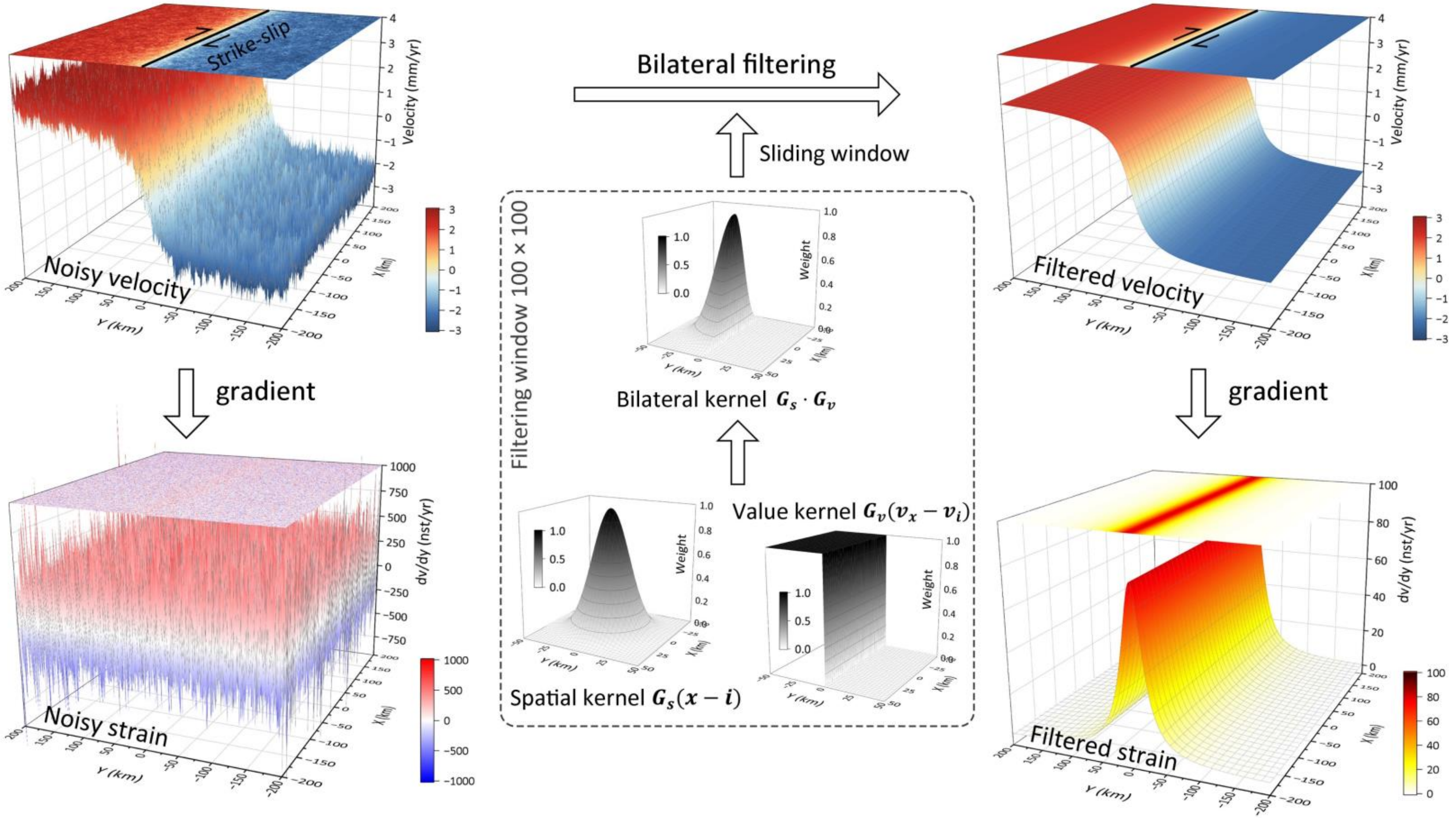

Schematic diagram of the bilateral filtering method and its influence on strain rate estimation

Development of **new InSAR velocity-field filter** that better recovers both magnitude and localization of on-fault strain rate.

$$G_s = \exp\left(-\frac{\| x - i \|^2}{2{\sigma_s}^2}\right)$$

Spatial kernel

$$G_v = \exp\left(-\frac{\| v(x) - v(i) \|^2}{2{\sigma_v}^2}\right)$$

Value kernel

$$v_{\mathrm{filtered}}(x) = \frac{1}{W_p} \sum_{i \in \mathcal{N}(x)} v(i) \cdot G_s(\| x - i \|) \cdot G_v(|v(x) - v(i)|)$$

POSTER SESSION II (Chang et al., 2026)

Strain Rate Comparison

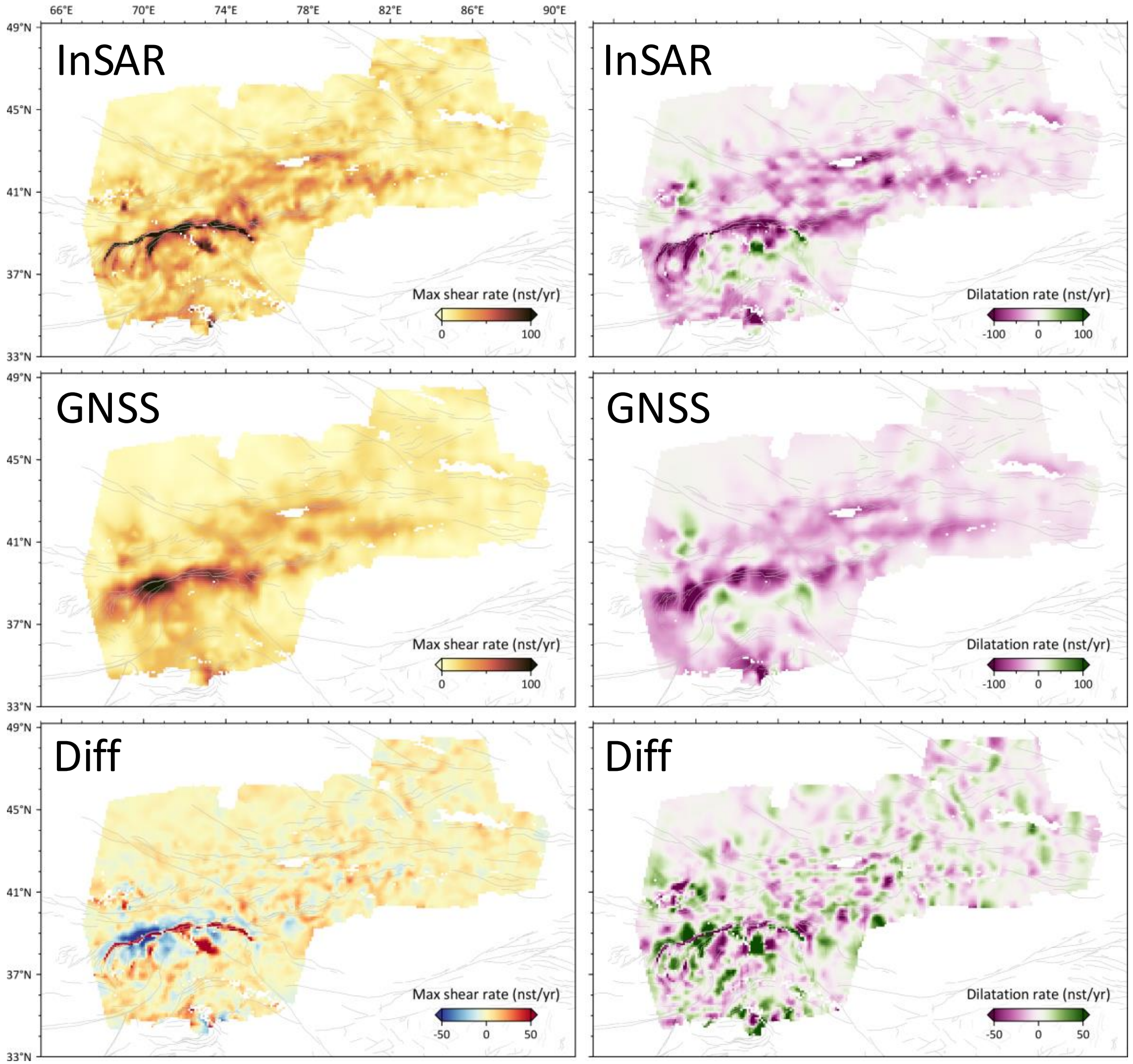

InSAR strain rate compare with **GNSS-only**

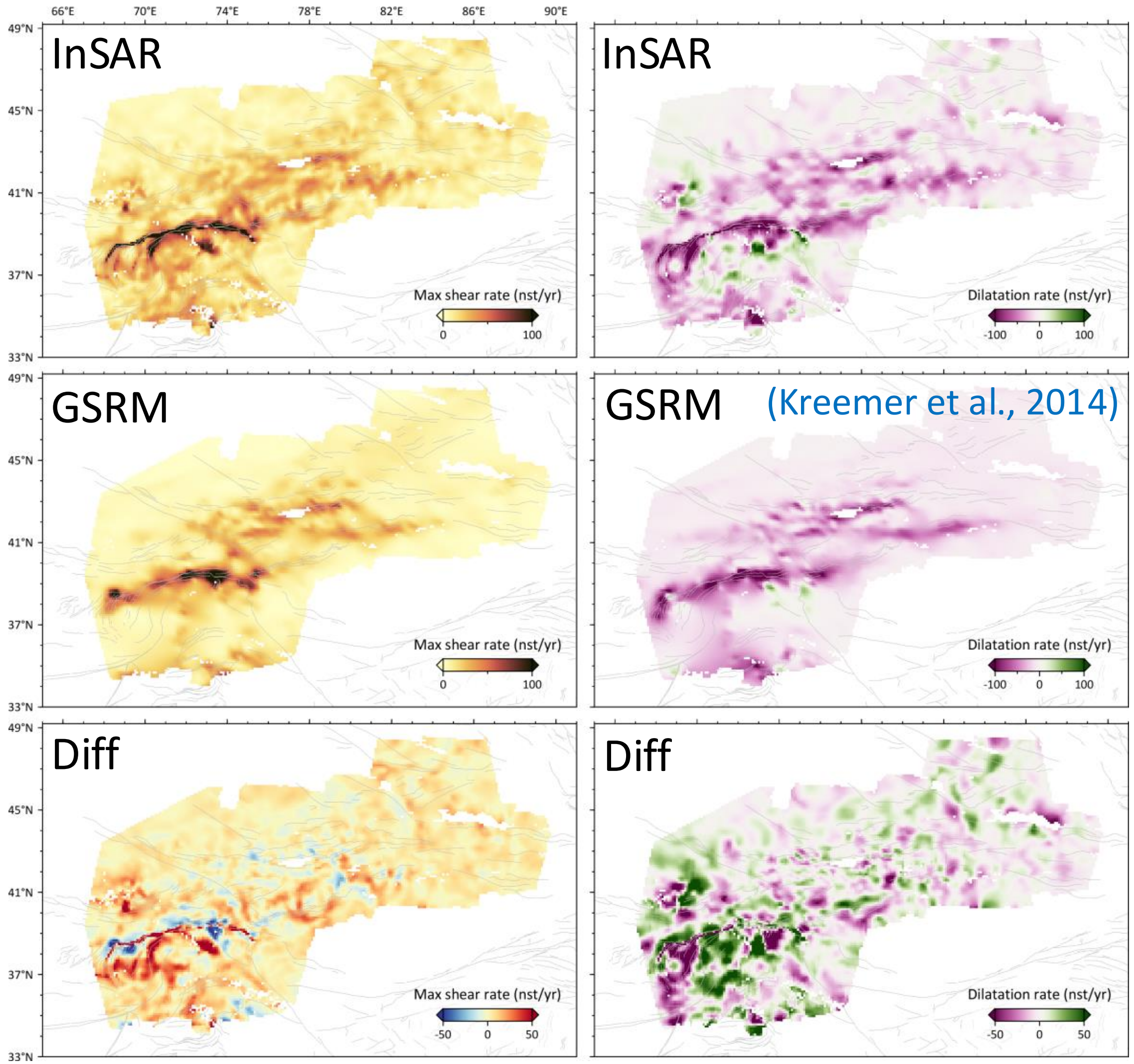

InSAR strain rate compare with **GSRM v2.1**

Fault Slip Deficit Rate Inversion

Strain-Rate-Based Inversion Avoids block partitioning, allows for systematic inversion of closely spaced faults (Johnson et al., 2024)

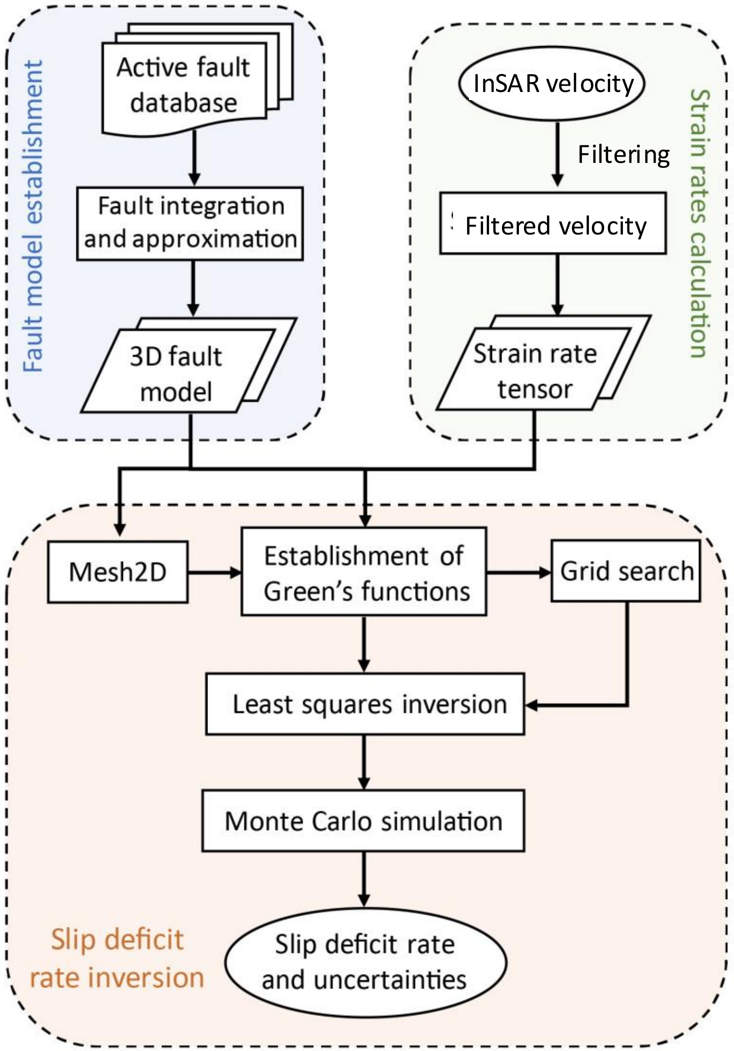

Workflow

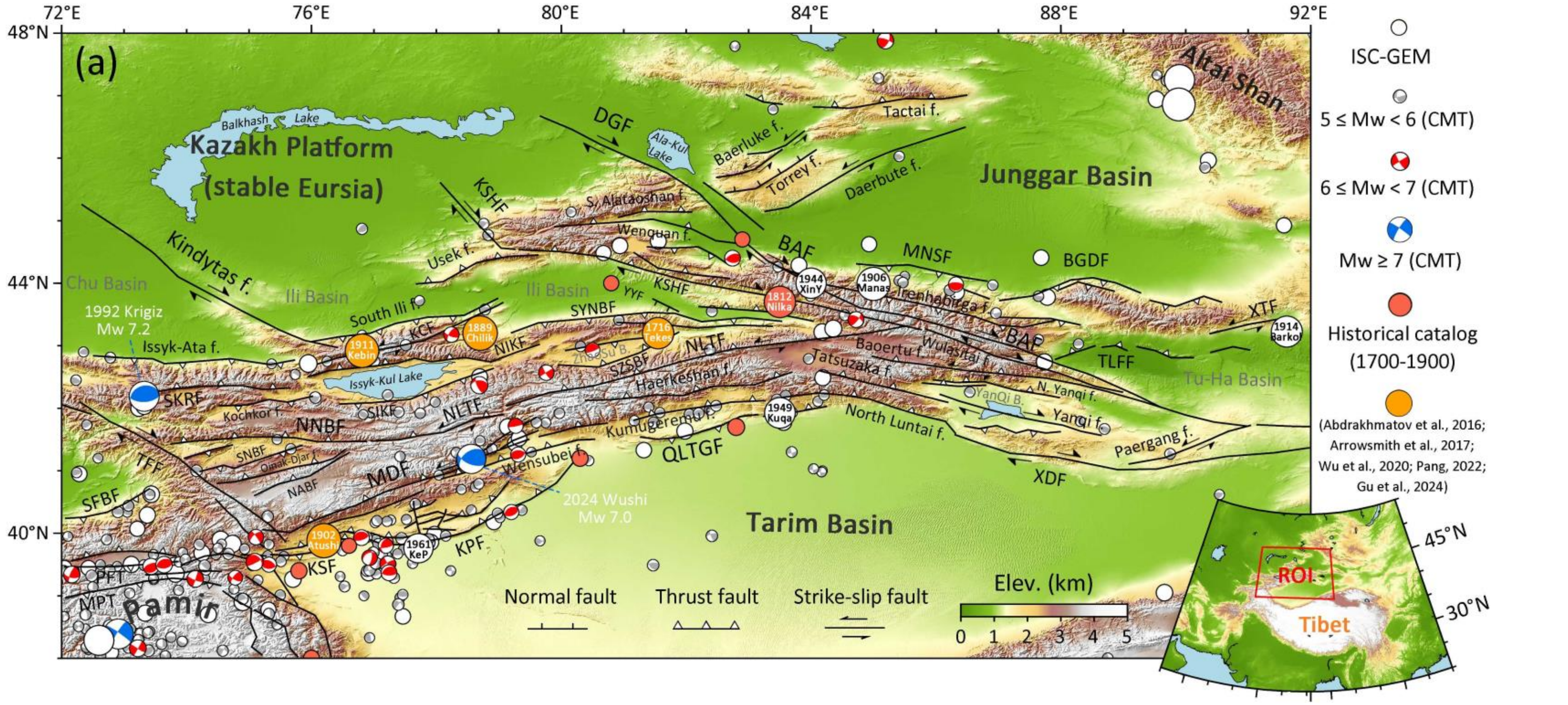

(Chang et al., 2025)

Fault database:

the China Active Faults Database, GEM global active faults database, and published studies.

Earthquake catalog:

ISC-GEM (1904-2024), GCMT (1976-2024), the China Historical Earthquake Catalog (1700-1900), and paleoseismological studies.

Fault Slip Deficit Rate

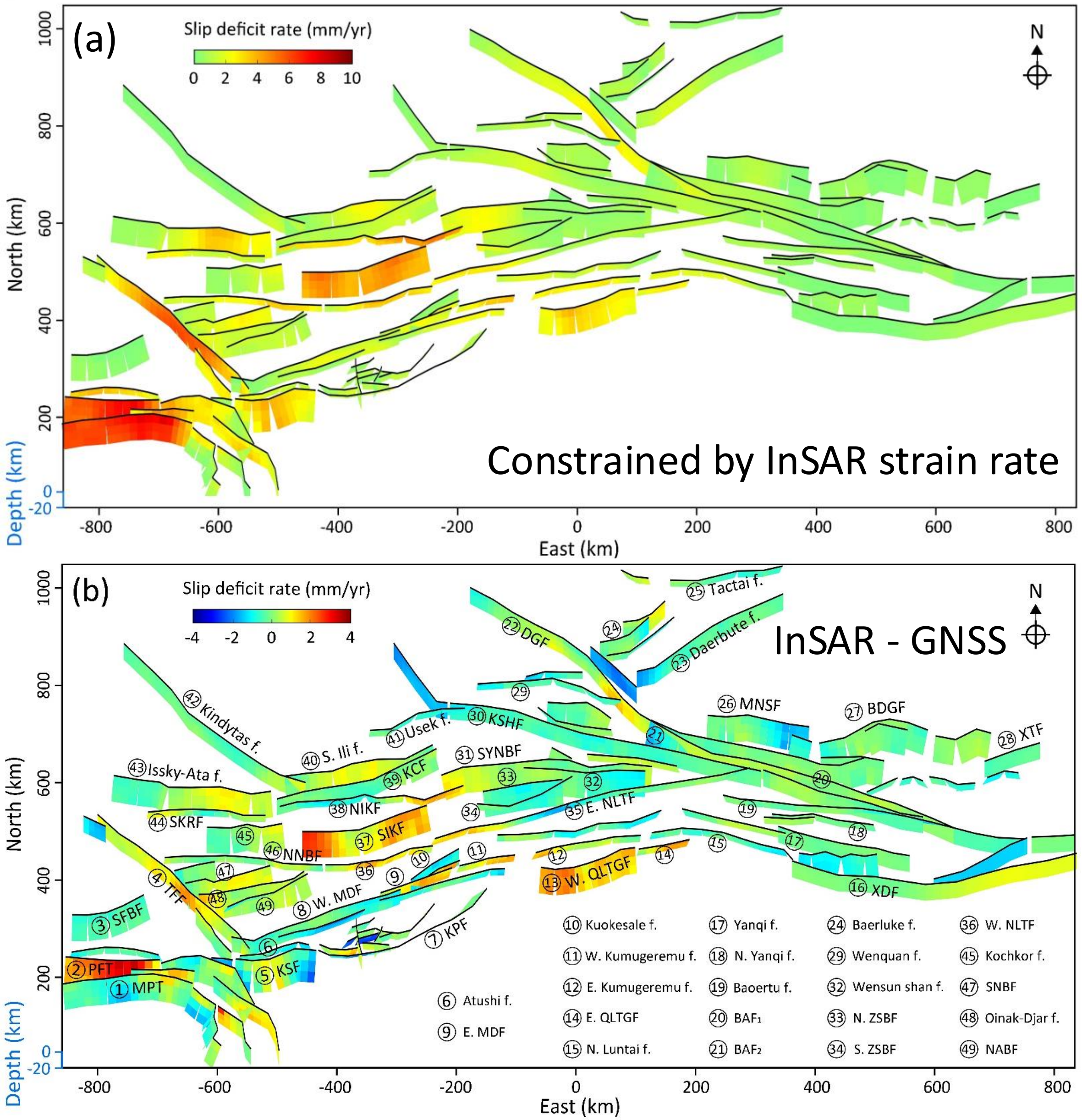

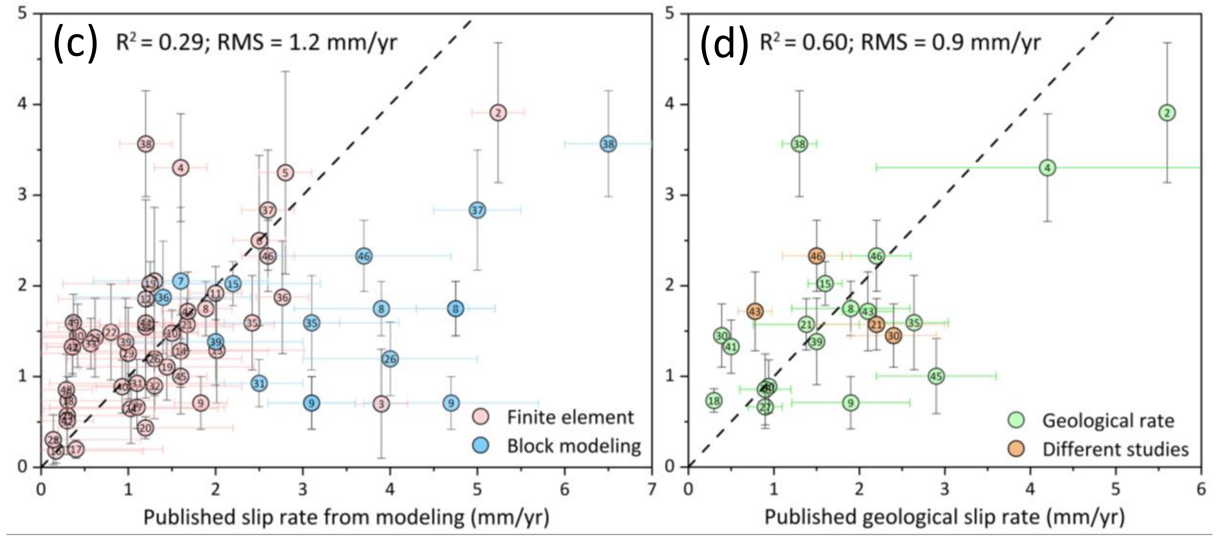

- InSAR strain rates reveal more details about fault slip deficit.
- Discrepancies may arise from differences in fault system simplifications, spatial limitations in geological rate measurements, timescale dependent variations in fault behavior.
- ~60% of strain rate is accommodated by major faults (interseismic coupling), while the remaining is associated with distributed moment sources (diffuse crustal deformation).

Seismic Moment Accumulation

Assumptions:

Elastic energy accumulated since the last major earthquake.

For segments without documented seismic events, we set the accumulation start time to 1700 (lower bound).

For earthquakes lacking precise location constraints, we associate them with the nearest mapped fault.

20 out of 439 fault segments are capable of generating Mw ≥ 7.0 earthquakes.

Uncertainties:

- Simple fault geometry (segmentation, dip, rake).
- Incompleteness of historical earthquake records.
- Fault intersection, cascading ruptures.
- Strain uncertainties from GNSS Interpolation (north).

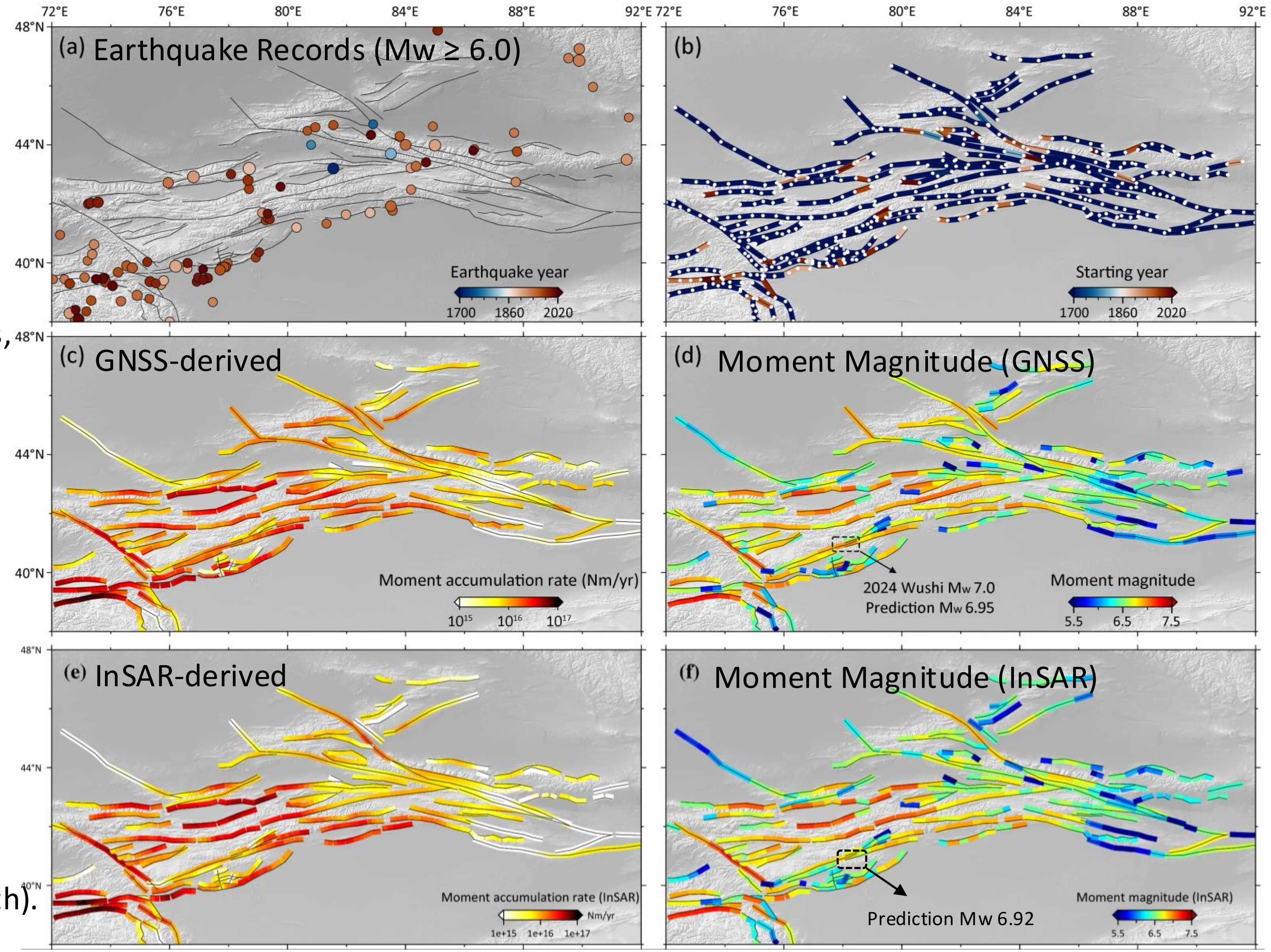

Deformation Dynamics

UNIVERSITY OF LEEDS

COMET

What controls the present-day deformation of Tianshan?

2D (Vertical averaged) Viscous Shell Model

(Houseman et al., 1986)

Downsample to 50 km (836 observations)

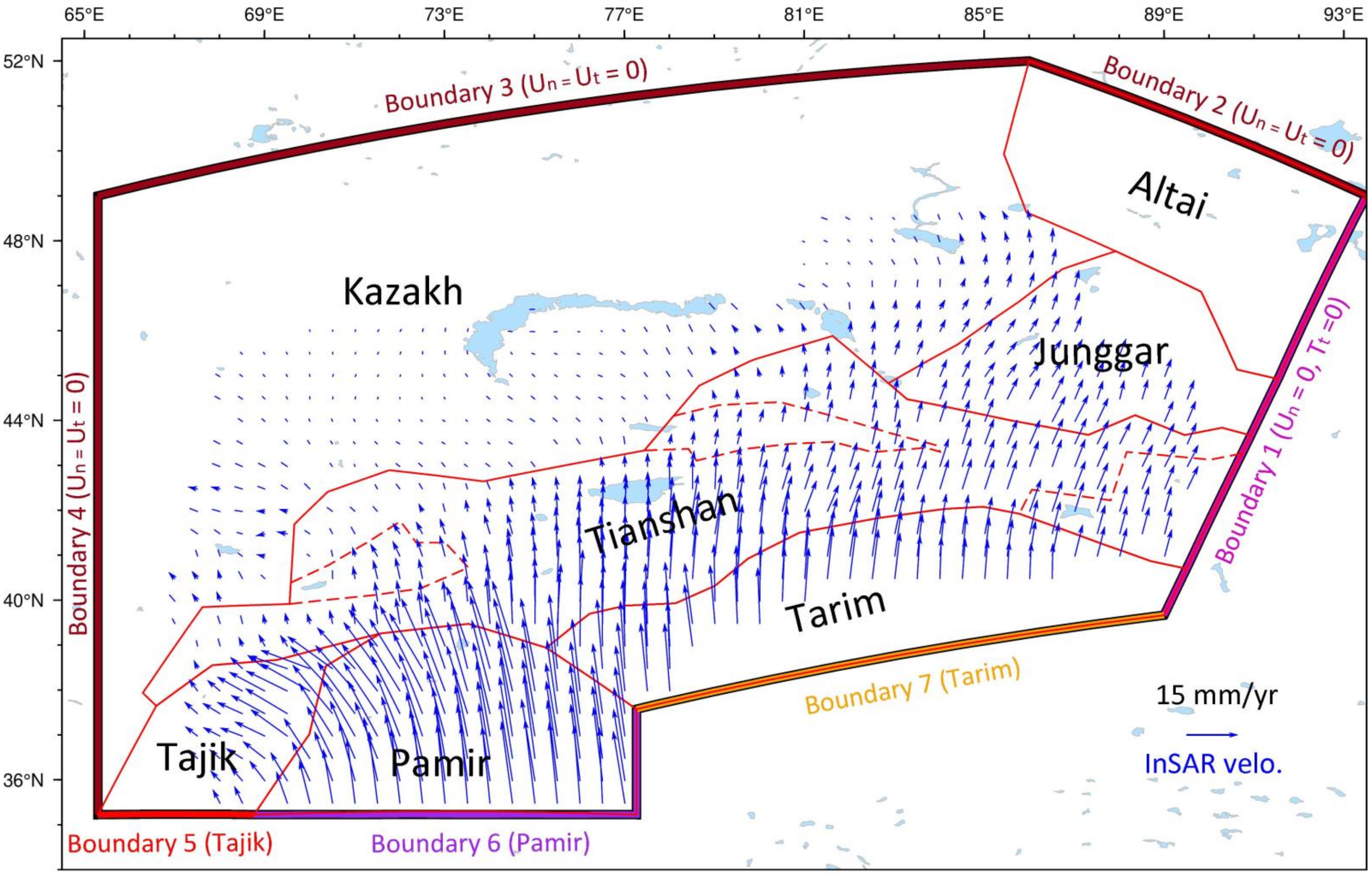

Boundary Conditions

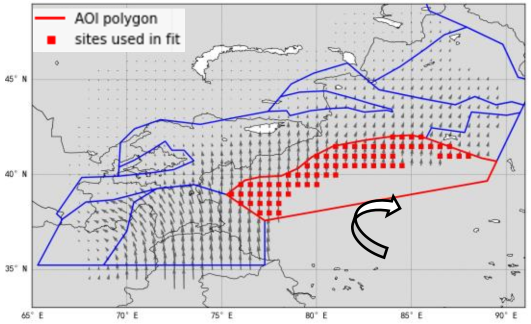

Tarim boundary:

Euler pole: 95.7E 38.7N

-0.68 deg/Myr

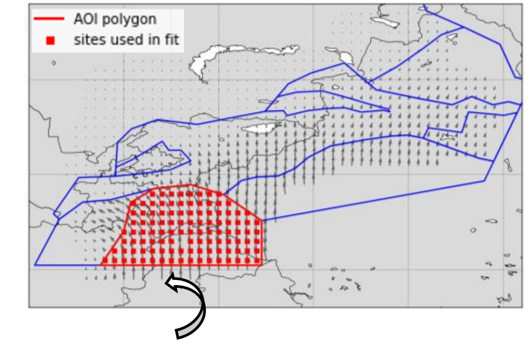

Pamir boundary :

Euler pole: 59.5E 33.0N

0.84 deg/Myr

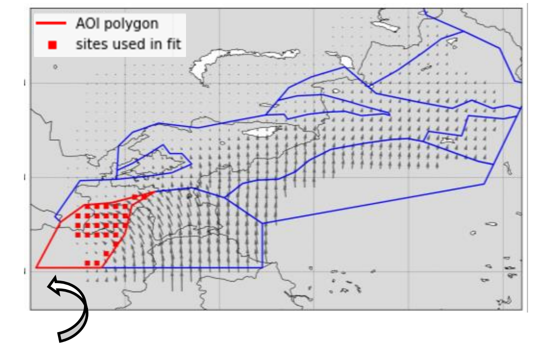

Tajik boundary:

Euler pole: 66.4E 34.8N

1.65 deg/Myr

Different Model Settings

Case1: Uniform strength

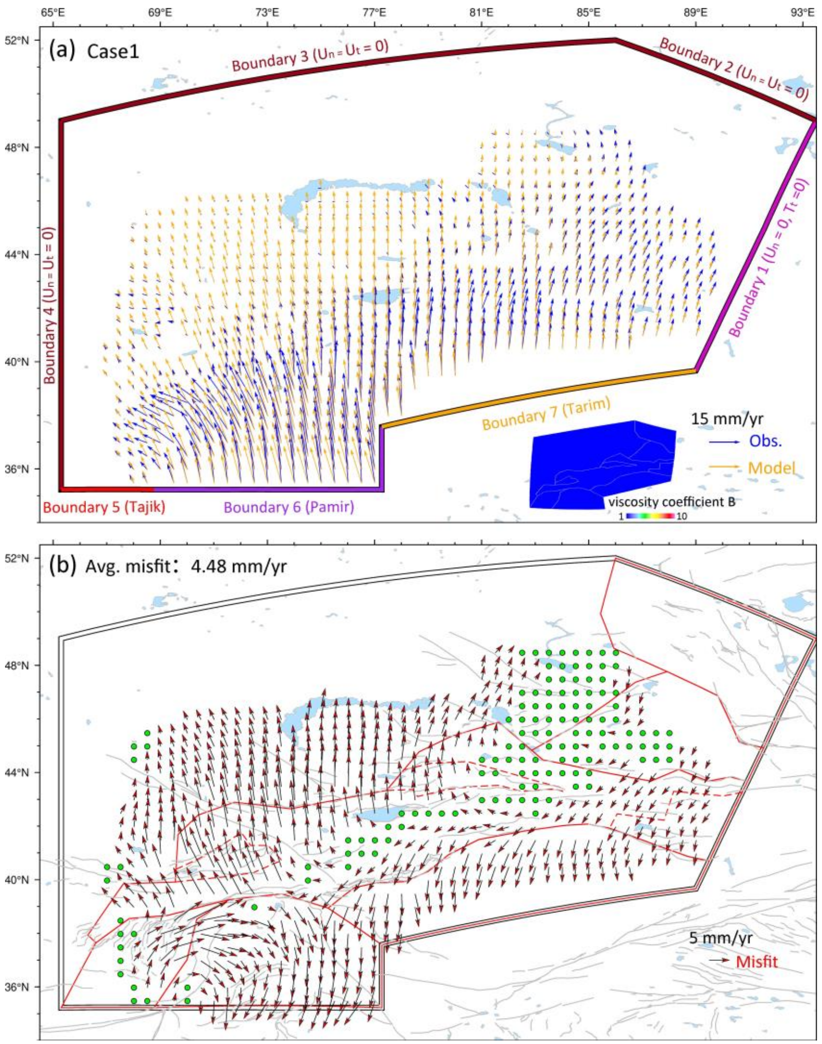

Case2: Variable strength (Optimal Param.)

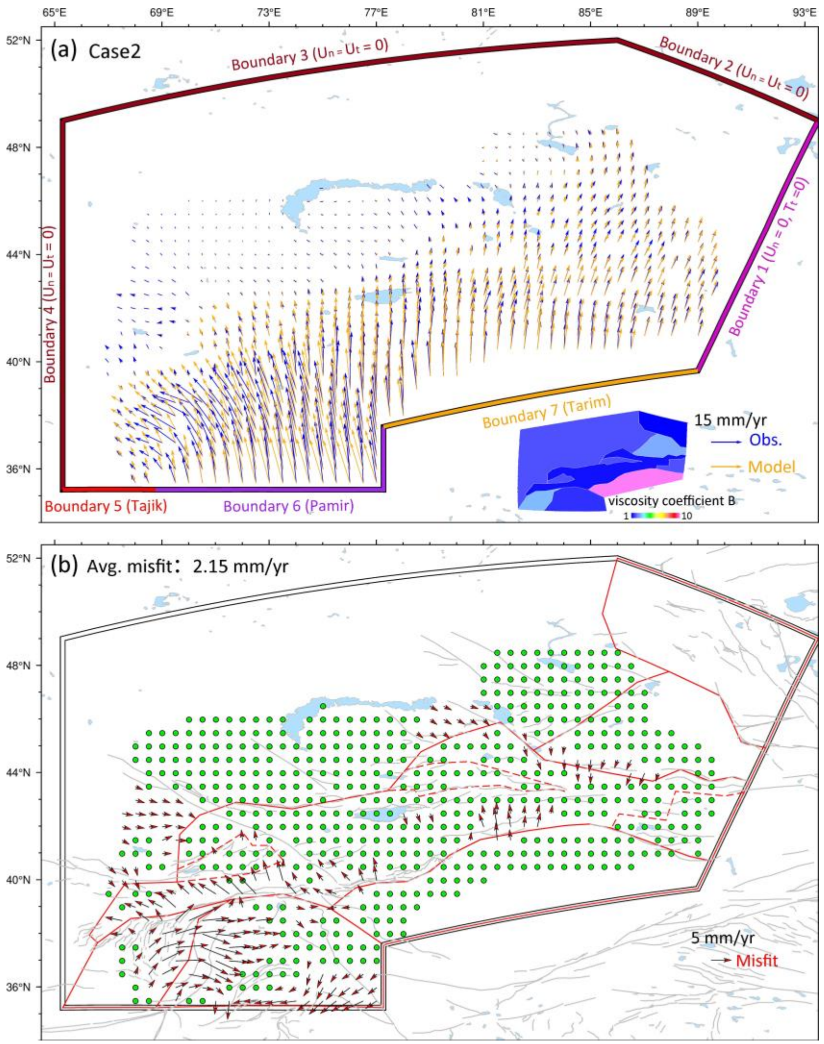

Case3: Add fault (ft and fn)

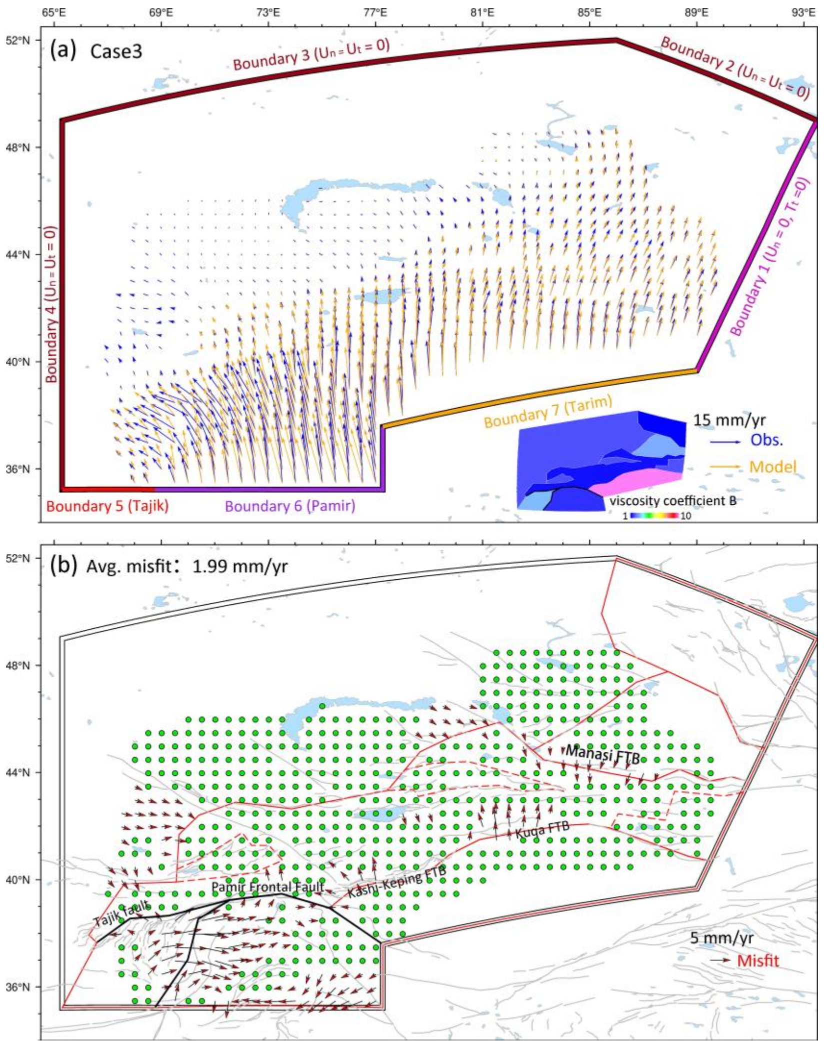

Model Comparison

East velocity

Case1 (uniform strength)

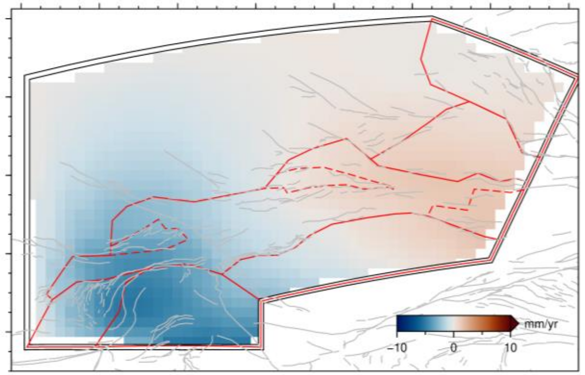

Case2 (variable strength)

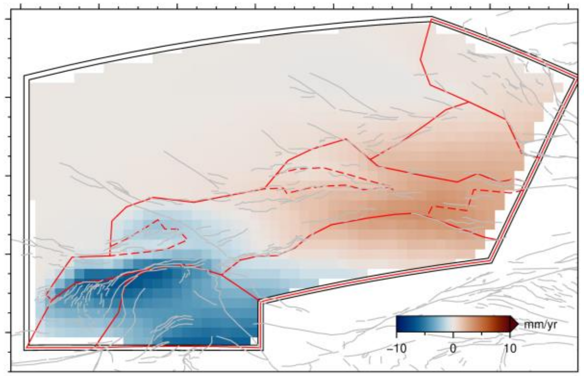

Case3 (Add fault)

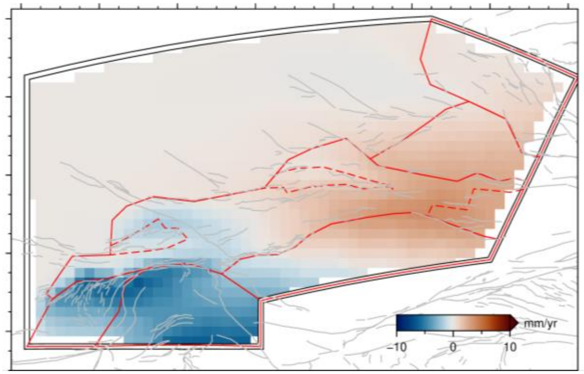

Observation

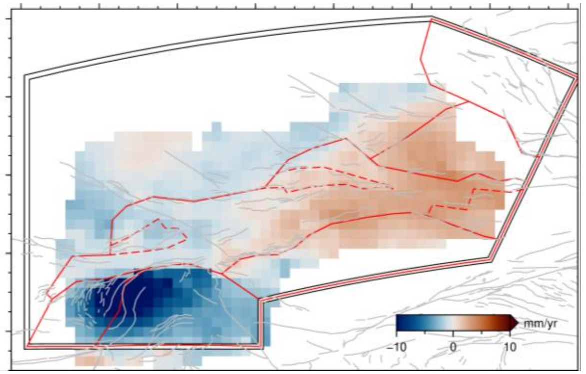

Main misfits are concentrated in the Pamir and Tajik

North velocity

Case1 (uniform strength)

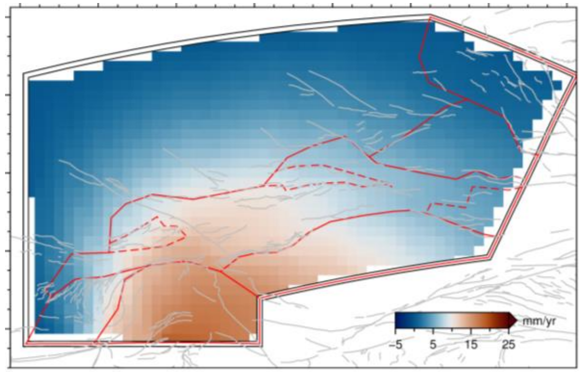

Case2 (variable strength)

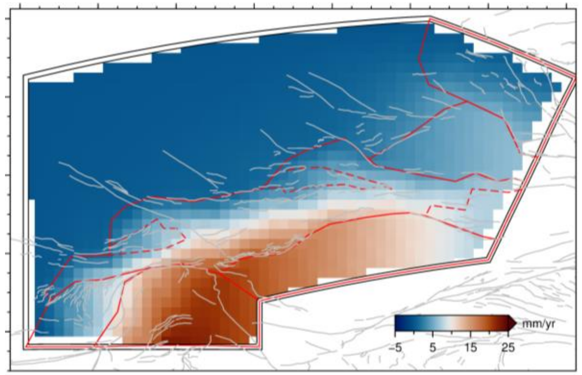

Case3 (Add fault)

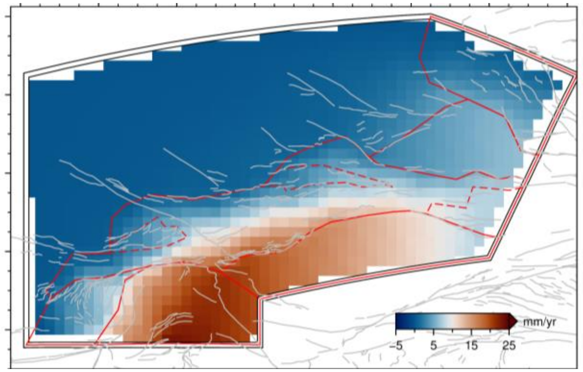

Observation

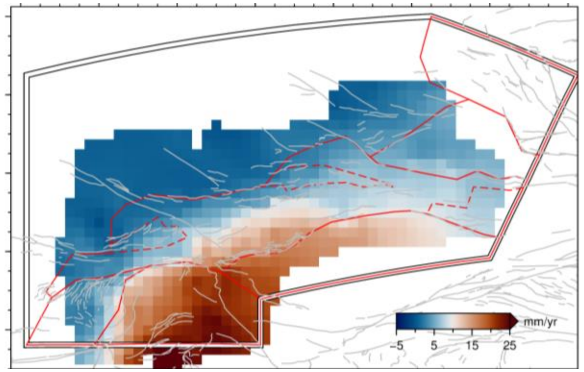

Deformation Dynamics

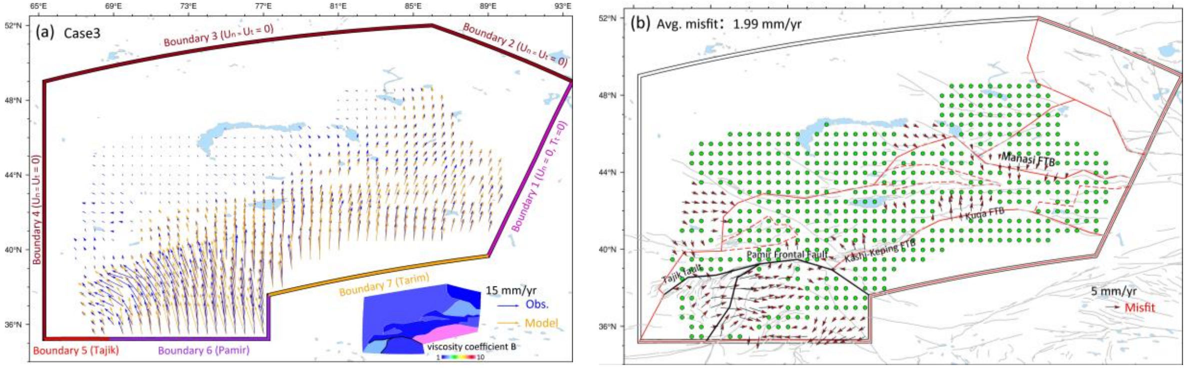

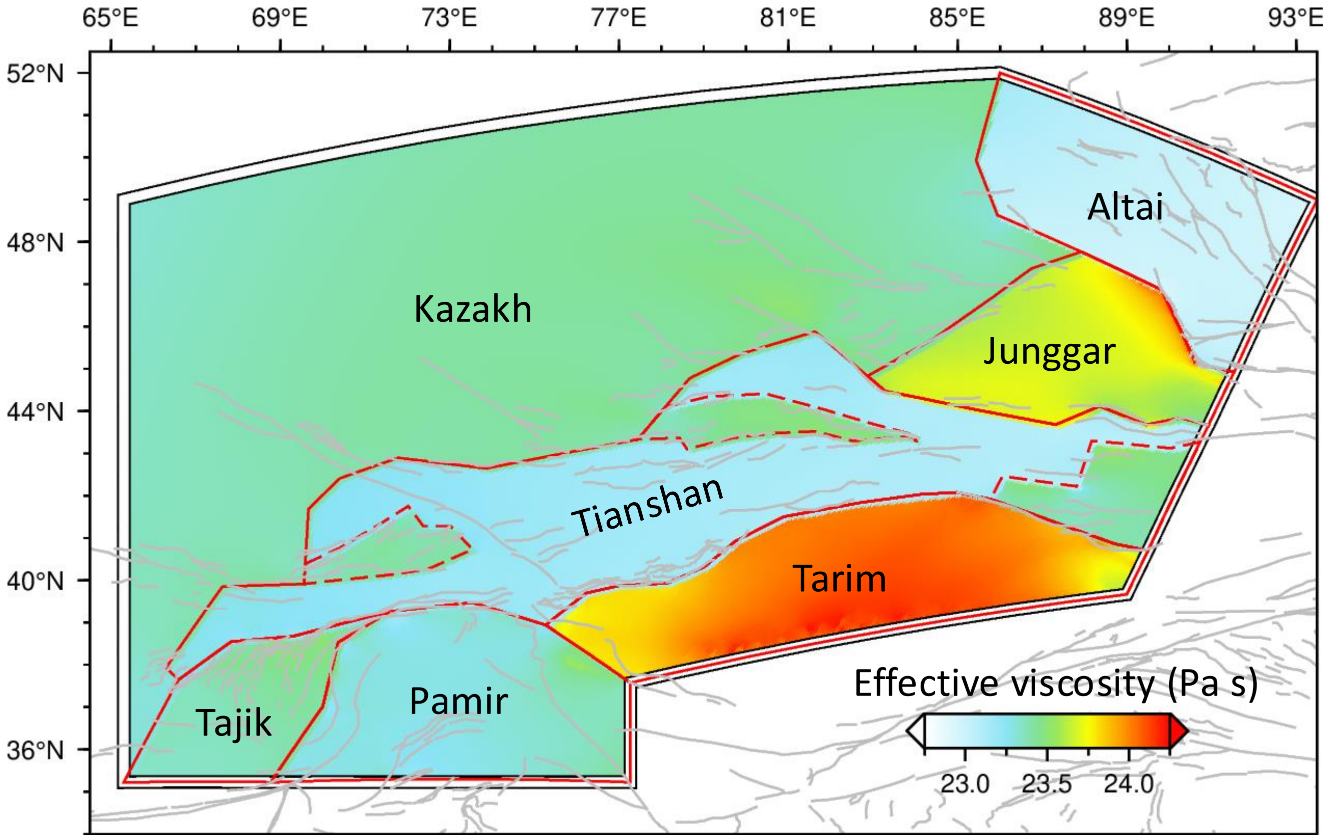

- Indentation of the Tarim and Pamir (boundary loading) is the first-order drivers of present-day deformation in the Tianshan.
- A relatively weak Tianshan lithosphere (depth-averaged 10^{23}Pa·s) is required to reproduce the observed deformation pattern; the effective viscosity is 2–10 times lower than that of the surrounding Kazakh and Tarim.

Next step:

- GPE is not a necessary factor for explaining the present-day deformation, further investigation is needed.
- The larger misfit near the Pamir-Tajik may be related to the plate subduction process; consider adding additional horizontal traction to the model.
- Further increase the model complexity and observational resolution to investigate rheological differences within the Tianshan.

Take-home messages

COMET

UNIVERSITY OF LEEDS

- A high-resolution three-dimensional interseismic surface velocity field covering approximately 2 million km^2 of the Tianshan and its surrounding regions is constructed, providing a data foundation for a better understanding of continental deformation and seismic hazards.

- Slip-deficit rates of 97 active faults in the Tianshan are systematically inverted from surface strain-rate constraints, and the interseismic elastic moment budget and future seismic potential of these faults are evaluated. 20 active fault segments have accumulated sufficient elastic strain energy to generate earthquakes of $M_w \geq 7.0$.

- Indentation of the Tarim and Pamir is the first-order dynamic drivers of present-day deformation; A relatively weak Tianshan lithosphere is required; gradients in lithospheric GPE are not necessary for explaining the present-day deformation; Weak fault primarily modulates the local velocity gradient.

xhfk9298@leeds.ac.uk; cfn@smail.nju.edu.cn

Actively looking for a postdoc position (Oct. 2026)

(Chang et al., 2025)

(Chang et al., 2026)